

# Chemotaxis increases metabolic exchanges between marine picophytoplankton and heterotrophic bacteria

Received: 5 April 2022

Accepted: 9 January 2023

Published online: 09 February 2023

 Check for updates

Jean-Baptiste Raina<sup>1,12</sup>✉, Marco Giardina<sup>1,12</sup>, Douglas R. Brumley<sup>1,2,12</sup>, Peta L. Clode<sup>3,4,5</sup>, Mathieu Pernice<sup>1</sup>, Paul Guagliardo<sup>1,3</sup>, Jeremy Bougoure<sup>3</sup>, Himasha Mendis<sup>6</sup>, Steven Smriga<sup>7</sup>, Eva C. Sonnenschein<sup>1,8,9</sup>, Matthias S. Ullrich<sup>10</sup>, Roman Stocker<sup>11</sup> & Justin R. Seymour<sup>1</sup>✉

Behaviours such as chemotaxis can facilitate metabolic exchanges between phytoplankton and heterotrophic bacteria, which ultimately regulate oceanic productivity and biogeochemistry. However, numerically dominant picophytoplankton have been considered too small to be detected by chemotactic bacteria, implying that cell–cell interactions might not be possible between some of the most abundant organisms in the ocean. Here we examined how bacterial behaviour influences metabolic exchanges at the single-cell level between the ubiquitous picophytoplankton *Synechococcus* and the heterotrophic bacterium *Marinobacter adhaerens*, using bacterial mutants deficient in motility and chemotaxis. Stable-isotope tracking revealed that chemotaxis increased nitrogen and carbon uptake of both partners by up to 4.4-fold. A mathematical model following thousands of cells confirmed that short periods of exposure to small but nutrient-rich microenvironments surrounding *Synechococcus* cells provide a considerable competitive advantage to chemotactic bacteria. These findings reveal that transient interactions mediated by chemotaxis can underpin metabolic relationships among the ocean's most abundant microorganisms.

The substantial impact of microbial communities on the productivity and biogeochemistry of the ocean is shaped by intricate networks of inter-organismal interactions<sup>1,2</sup>. Among pelagic microbial relationships, the often-mutualistic metabolic associations between phytoplankton

and bacteria are some of the most important<sup>3,4</sup>. Reciprocal exchanges of metabolites, including a diverse suite of organic and inorganic molecules, vitamins and minerals can support the growth of both phytoplankton and bacterial partners<sup>5–7</sup>. However, within the vast expanses of

<sup>1</sup>University of Technology Sydney, Climate Change Cluster, Faculty of Science, Ultimo, New South Wales, Australia. <sup>2</sup>School of Mathematics and Statistics, The University of Melbourne, Parkville, Victoria, Australia. <sup>3</sup>Centre for Microscopy Characterisation and Analysis, The University of Western Australia, Perth, Western Australia, Australia. <sup>4</sup>UWA School of Biological Sciences, The University of Western Australia, Perth, Western Australia, Australia.

<sup>5</sup>UWA Oceans Institute, The University of Western Australia, Perth, Western Australia, Australia. <sup>6</sup>Metabolomics Australia, Bio21 Institute, The University of Melbourne, Parkville, Victoria, Australia. <sup>7</sup>Department of Earth Atmospheric and Planetary Sciences, Massachusetts Institute of Technology, Cambridge, MA, USA. <sup>8</sup>Department of Biotechnology and Biomedicine, Technical University of Denmark, Kgs. Lyngby, Denmark. <sup>9</sup>Department of Biosciences, Swansea University, Singleton Park, Swansea, UK. <sup>10</sup>Department of Life Sciences & Chemistry, Jacobs University Bremen, Bremen, Germany. <sup>11</sup>Institute of Environmental Engineering, Department of Civil, Environmental and Geomatic Engineering, ETH Zurich, Zurich, Switzerland. <sup>12</sup>These authors contributed equally: Jean-Baptiste Raina, Marco Giardina, Douglas R. Brumley. ✉e-mail: [Jean-Baptiste.Raina@uts.edu.au](mailto:Jean-Baptiste.Raina@uts.edu.au); [Justin.Seymour@uts.edu.au](mailto:Justin.Seymour@uts.edu.au)

the ocean, the efficacy of these chemical exchanges will be hindered by large inter-cell distances (hundreds of micrometres on average) and the sharp diffusive decay of metabolite concentrations with distance from exuding cells<sup>8</sup>. Phytoplankton–bacteria partnerships may, nevertheless, overcome these constraints through the formation of close spatial associations within the microenvironment immediately surrounding individual phytoplankton cells, known as the phycosphere<sup>9</sup>, which is characterized by elevated concentrations of metabolites emanating from the phytoplankton cell. It has long been theorized<sup>9–11</sup> that bacteria can locate and maintain position within the phycosphere using chemotaxis—the capacity of motile cells to migrate up or down chemical gradients—resulting in sustained spatial proximity of partners<sup>12</sup> and greatly enhanced metabolic exchanges<sup>13</sup>.

There is substantial evidence for bacterial chemotaxis towards phytoplankton-derived chemicals<sup>9,12,14,15</sup> and for the ability of bacteria to use chemotaxis to actively aggregate around large phytoplankton cells, such as diatoms<sup>16</sup>. Yet, across vast areas of the ocean, phototrophic biomass and primary production are dominated by picophytoplankton (<3 µm), including picoeukaryotes and the cyanobacteria *Prochlorococcus* and *Synechococcus*<sup>17</sup>. Like large phytoplankton including diatoms and dinoflagellates, these picophytoplankton appear to have important metabolic interdependencies with heterotrophic bacteria. Laboratory cultures of *Prochlorococcus* and *Synechococcus* exhibit enhanced growth in the presence of specific heterotrophic associates<sup>18–20</sup>, and metabolic exchanges have been identified using transcriptomic and proteomic approaches<sup>18,21</sup>. However, the nature of the ecological coupling between picophytoplankton and heterotrophic bacteria in the environment is somewhat paradoxical. While close proximity of partners is anticipated to strongly enhance and sustain mutualistic phototroph–heterotroph interactions<sup>12</sup>, physical constraints associated with the small size of *Prochlorococcus* and *Synechococcus* cells are thought to prevent heterotrophic bacteria from using chemotaxis to detect and retain position within their phycosphere<sup>22</sup>. In this Article, we show, however, that heterotrophic bacteria are indeed able to utilize chemotaxis to substantially enhance their metabolic exchanges with picophytoplankton, demonstrating that behavioural associations may shape the ecological relationships among some of the oceans' most abundant microorganisms.

## Results

### *Synechococcus* and *Marinobacter* exchange N and C

Using nano-scale secondary ion mass spectrometry (NanoSIMS), we directly quantified the chemical exchanges between *Synechococcus* strain CS-94 RRIMP N1 and *Marinobacter adhaerens* HP15, a heterotrophic Gammaproteobacterium associated with larger phytoplankton (diatoms)<sup>13,23</sup>. Closely related *M. adhaerens* strains (more than 98% 16S ribosomal RNA gene sequence identity) are also abundant in picophytoplankton cultures<sup>20,24</sup>. Given that *Synechococcus* cells produce and release nitrogen-rich dissolved organic matter (DOM) that can be utilized by heterotrophic bacteria<sup>18</sup>, we tracked the transfer of nitrogen from *Synechococcus* to *M. adhaerens*. *Synechococcus* cells were grown in f/2 medium with <sup>15</sup>N-labelled NaNO<sub>3</sub> as the only source of nitrogen for 1 week before experiments, to ensure high levels of <sup>15</sup>N enrichment in cells. To facilitate cell localization under NanoSIMS<sup>25</sup>, *M. adhaerens* cells were grown separately with <sup>13</sup>C-labelled amino acids. *Synechococcus* and *M. adhaerens* cells were then thoroughly washed to remove isotopic labels from suspensions and co-grown across a range of *Synechococcus* concentrations (10<sup>3</sup>, 10<sup>4</sup> and 10<sup>5</sup> cells ml<sup>-1</sup>) reflecting those occurring in different environments (from open ocean to coastal waters), with a constant concentration of *M. adhaerens* (10<sup>6</sup> cells ml<sup>-1</sup>). Following 3 h of co-incubation in stable light and temperature conditions<sup>26</sup>, samples were collected for NanoSIMS analysis.

After co-incubation, *M. adhaerens* cells were enriched in <sup>15</sup>N derived from *Synechococcus*, with levels up to 2.7 times the natural abundance

values of <sup>15</sup>N in unlabelled *M. adhaerens* (<sup>15</sup>N/<sup>14</sup>N = 0.010 ± 0.00081, n = 172, compared with 0.0037 ± 0.000046, n = 300). Significant uptake of *Synechococcus*-derived <sup>15</sup>N by *M. adhaerens* (the percentage of N incorporated into the cells relative to the initial N content; see equation (1) in Methods) occurred at all *Synechococcus* concentrations (Kruskal–Wallis (KW), P < 0.05; Supplementary Table 1). <sup>15</sup>N uptake in *M. adhaerens* increased strongly with the concentration of *Synechococcus* cells (KW, P < 0.05; Supplementary Table 1), from 0.36% at 10<sup>3</sup> *Synechococcus* cells ml<sup>-1</sup> to 0.98% at 10<sup>5</sup> *Synechococcus* cells ml<sup>-1</sup> (Fig. 1a,b). These results deliver direct evidence that nitrogen-containing compounds exuded from *Synechococcus* are taken up by heterotrophic bacteria, demonstrating that chemical exchange takes place between these two organisms.

To identify which organic nitrogen compounds are exuded by *Synechococcus*, we used an untargeted metabolomic approach. We identified 34 nitrogen-containing compounds exuded by *Synechococcus*, using gas chromatography coupled with mass spectrometry (GC–MS). The exuded compounds included amino acids (cysteine, phenylalanine, methionine and leucine), amines (tyramine and ethanolamine), amides (urea), vitamins (nicotinamide and pantothenic acid) and purines (xanthine; Supplementary Table 2). Notably, an analysis of the *M. adhaerens* HP15 genome<sup>27</sup> indicates that this bacterium has the capacity to catabolize at least 24 of these 34 compounds (>70%; Supplementary Table 2), highlighting the probable importance of these molecules in the metabolic exchange between *Synechococcus* and heterotrophs<sup>18</sup>.

Beyond the transfer of nitrogen from *Synechococcus* to *M. adhaerens*, our analysis also revealed an unexpected exchange of carbon from *M. adhaerens* to *Synechococcus*, evidenced by <sup>13</sup>C enrichment in *Synechococcus* cells that reached up to 2.9 times the natural abundance values in unlabelled cells (<sup>13</sup>C/<sup>12</sup>C = 0.032 ± 0.0051, n = 10, compared with 0.011 ± 0.000027, n = 102). <sup>13</sup>C uptake was not affected by the *Synechococcus* concentration (the percentage of C incorporated into the cells relative to the initial C content; see equation (1) in Methods; KW, P > 0.05; Supplementary Table 3 and Fig. 1c,d), probably because no competition for <sup>13</sup>C occurred at the *Synechococcus* concentrations tested (Methods). Using GC–MS, we identified 80 organic compounds exuded by *M. adhaerens* that potentially contributed to the carbon enrichment in *Synechococcus*. These compounds included sugars (galactose, mannose and sucrose), amino acids (glycine, alanine and serine), organic acids (phosphoric acid, benzoic acid and pyroglutamic acid), hormones (methoxytryptamine) and fatty acids (linoleic acid, palmitic acid and myristic acid; Supplementary Table 4). The identity of some of these compounds is consistent with previous reports of photoheterotrophy in *Synechococcus* and their uptake of amino acids and urea<sup>28,29</sup>. Taken together, these results provide the first direct evidence that *Synechococcus* cells can simultaneously supply heterotrophic bacteria with nitrogen while acquiring carbon from them (Fig. 1e), pointing to a relationship that is akin to the reciprocal metabolic associations observed between larger phytoplankton (for example, diatoms) and heterotrophic bacteria<sup>6</sup>.

### Chemotaxis facilitates reciprocal metabolic exchanges

*M. adhaerens* is motile<sup>13</sup>, and we found, using a chemotaxis assay<sup>30</sup>, that it is significantly attracted towards DOM exuded by *Synechococcus* (3.5 ± 0.3 times more cells compared with controls, which is consistent with levels of chemoattraction reported for other marine Gammaproteobacteria in the same experimental conditions<sup>31</sup>; analysis of variance (ANOVA), P < 0.05; Supplementary Table 5 and Extended Data Fig. 1). However, this observation does not provide confirmation that *M. adhaerens* can use chemotaxis to home in on the phycosphere of individual *Synechococcus* cells to gain a metabolic benefit. In fact, a previous mathematical model (parameterized with the chemosensory capabilities of *Escherichia coli*), predicted that the chemical gradients in the phycosphere of picophytoplankton are too small to

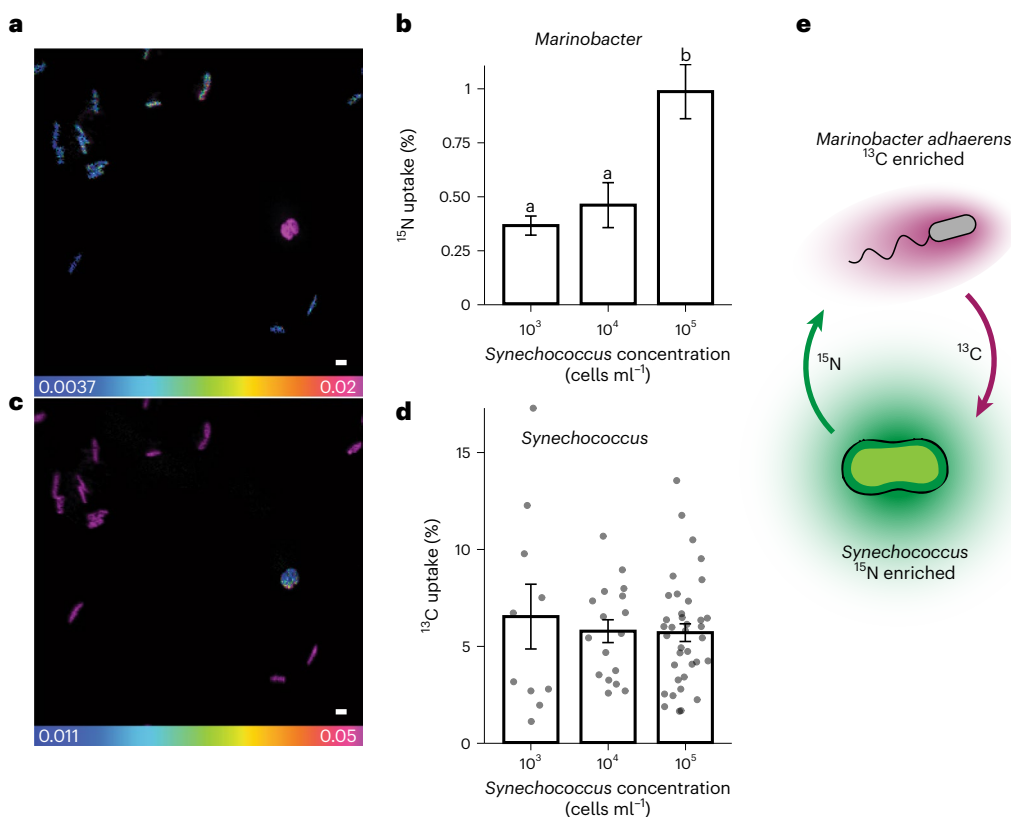


**Fig. 1 | Reciprocal exchanges between *Synechococcus* and *M. adhaerens***  
**HP15.** **a**, Representative <sup>15</sup>N/<sup>14</sup>N ratio image using NanoSIMS (highlighting the highly enriched *Synechococcus* cell, pink; at least 20 images were acquired per treatment; scale bar, 1 μm). **b**, <sup>15</sup>N uptake of *M. adhaerens* HP15 WT originating from *Synechococcus* ( $10^3$ :  $n = 166$ ;  $10^4$ :  $n = 286$ ;  $10^5$ :  $n = 172$ ). **c**, Representative <sup>13</sup>C/<sup>12</sup>C ratio image using NanoSIMS (identifying highly enriched *M. adhaerens* cells, pink; at least 20 images were acquired per treatment; scale bar, 1 μm).

**d**, <sup>13</sup>C uptake in *Synechococcus* cells originating from *M. adhaerens* ( $10^3$ :  $n = 10$ ;  $10^4$ :  $n = 17$ ;  $10^5$ :  $n = 37$ ), at different *Synechococcus* concentrations. **e**, Reciprocal exchange of chemical currencies through diffusion in the bulk. Stable isotope uptake from **b** and **d** were calculated according to ref. <sup>46</sup> (see equation (1) in Methods). Error bars in **b** and **d** represent standard error of the mean. Significant differences (KW) are indicated by using different letters; see also Supplementary Tables 1 and 3. The full distribution of the data is shown in Extended Data Fig. 9.

be detectable by chemotactic bacteria<sup>22</sup>. This prediction has resulted in the paradigm that, whereas associations between heterotrophic bacteria and large phytoplankton can be mediated by bacterial behaviour<sup>11,22</sup>, those between heterotrophic bacteria and picophytoplankton cannot<sup>22</sup>. To explicitly test the role of chemotaxis in the exchange of resources between the two microorganisms, we compared the uptake of *Synechococcus*-derived <sup>15</sup>N by *M. adhaerens* among three *M. adhaerens* phenotypes: the motile and chemotactic wild type (WT); a motile but non-chemotactic mutant ( $\Delta cheA$ )<sup>13</sup>; and a non-motile mutant ( $\Delta fliC$ )<sup>13</sup> (Fig. 2a).

These experiments revealed that the magnitude of the chemical exchange between *Synechococcus* and *M. adhaerens* was substantially smaller when *M. adhaerens* cells were not chemotactic (importantly, no cell attachment was observed between the two bacterial species in any of the treatments). After 3 h of co-incubation with <sup>15</sup>N-labelled *Synechococcus*, bacteria from all three phenotypes were enriched in <sup>15</sup>N compared with unlabelled cells (Fig. 2b), but the level of enrichment was strongly determined by the bacteria's capacity for chemotaxis. Specifically, in the treatments with the low and intermediate *Synechococcus* concentrations ( $10^3$  and  $10^4$  cells ml<sup>-1</sup>), the <sup>15</sup>N uptake of the WT *M. adhaerens* was more than double that of the  $\Delta fliC$  (2.6- and 2.4-fold increase, for  $10^3$  and  $10^4$  cells ml<sup>-1</sup>, respectively) and  $\Delta cheA$  (2.0- and 1.8-fold increase, for  $10^3$  and  $10^4$  cells ml<sup>-1</sup>, respectively) mutants (KW,  $P < 0.05$ ; Fig. 2b and Supplementary Table 6). At high *Synechococcus* concentrations ( $10^5$  cells ml<sup>-1</sup>) this difference vanished, possibly because a high background concentration of substrates

renders chemotaxis less advantageous. These results overturn the paradigm that chemotaxis of heterotrophic bacteria towards picophytoplankton is not possible, showing instead that it can deliver bacteria with a substantial advantage in metabolic uptake.

Chemotaxis of *M. adhaerens* also influenced the uptake of *M. adhaerens*-derived carbon by *Synechococcus*. At concentrations of  $10^4$  and  $10^5$  cells ml<sup>-1</sup>, *Synechococcus* co-incubated with WT *M. adhaerens* were up to four times more enriched in <sup>13</sup>C than cells co-incubated with  $\Delta fliC$  (1.2- and 1.5-fold increase, for  $10^4$  and  $10^5$  cells ml<sup>-1</sup>, respectively) and  $\Delta cheA$  (1.8- and 4.4-fold increase, for  $10^4$  and  $10^5$  cells ml<sup>-1</sup>, respectively) mutants (KW,  $P < 0.001$ ; Fig. 2c and Supplementary Table 7). Therefore, chemotaxis by heterotrophic bacteria not only enhances the uptake of picophytoplankton-derived metabolites by the bacteria, but also increases picophytoplankton uptake of bacteria-derived metabolites, identifying chemotaxis as an important behaviour in the establishment of reciprocal resource exchange between two of the most numerous groups of microorganisms in the ocean.

#### Phycosphere interactions are short-lived yet repeated

The role of chemotaxis in enhancing bacterial uptake of picophytoplankton metabolites was supported by a mathematical model that simulates the motion of chemotactic bacteria in a three-dimensional DOM landscape representative of experimental conditions. A suspension of *Synechococcus* cells was modelled as a collection of randomly positioned spherical 'hotspots', each exuding DOM at a steady rate

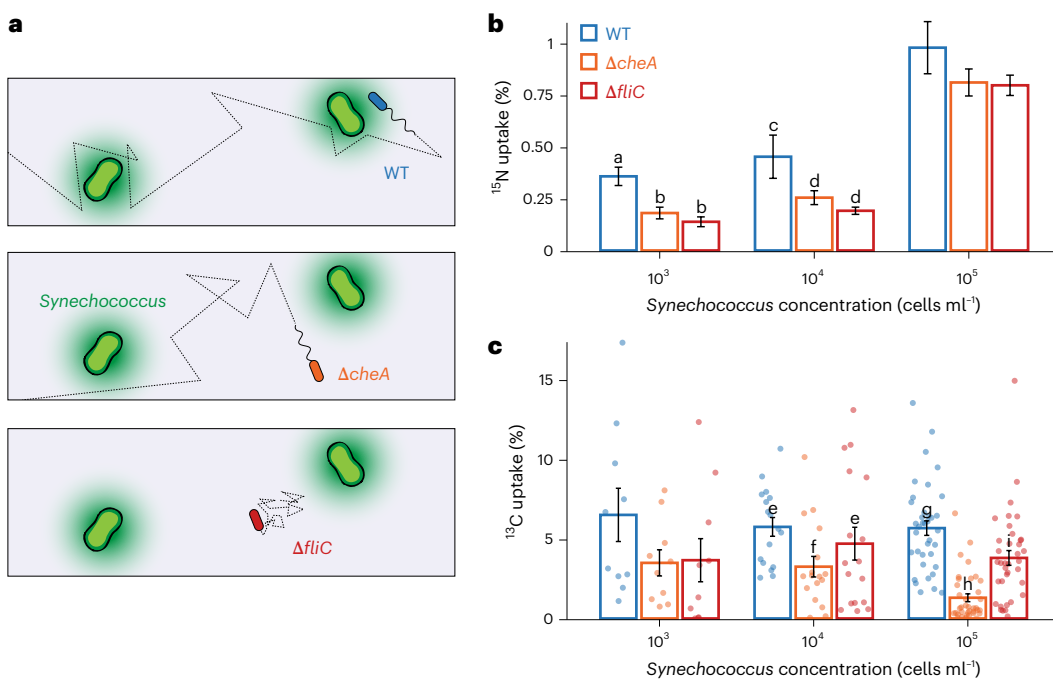


**Fig. 2 | Reciprocal exchanges between *Synechococcus* and *M. adhaerens* HP15 are enhanced by chemotaxis.** **a–c**, The chemotactic (WT), non-chemotactic ( $\Delta cheA$ ) and non-motile ( $\Delta fliC$ ) strains of *Marinobacter* interact with *Synechococcus* phycospheres in qualitatively different ways (**a**), resulting in strong differences in the  $^{15}\text{N}$  uptake of *M. adhaerens* ( $10^3$ :  $n = 166$ ;  $10^4$ :  $n = 286$ ;  $10^5$ :  $n = 172$ ) (**b**) and  $^{13}\text{C}$  uptake in *Synechococcus* ( $10^3$ :  $n = 10$ ;  $10^4$ :  $n = 17$ ;  $10^5$ :  $n = 37$ ) (**c**).

Error bars in **b** and **c** represent standard error of the mean. Significant differences (KW) are indicated using different letters (see also Supplementary Tables 6 and 7). Stable isotope uptake from **b** and **c** were calculated according to ref.<sup>46</sup> (see equation (1) in Methods). The full distribution of the data is shown in Extended Data Fig. 9.

$L = 0.052 \text{ pmol h}^{-1}$ , which was determined by calibrating the model with experimental parameters (Methods and Supplementary Table 8) and is consistent with predictions based on previous estimates of phytoplankton exudation rates<sup>12</sup>. Based on the high proportion of amino acids we detected in the *Synechococcus* exudates by metabolomics (Supplementary Table 2), the DOM was represented in the model as a single chemoattractant molecule of amino-acid size (diffusivity,  $608 \mu\text{m}^2 \text{s}^{-1}$ ) (ref. <sup>32</sup>). The model predicted how the DOM concentration changes in space and time as a result of exudation, diffusion and bacterial uptake, and used this information to compute the three-dimensional trajectories of bacteria executing run-reverse-flick locomotion representative of monothrixous marine bacteria<sup>22,32</sup>. The amount of DOM taken up by 500 individual *M. adhaerens* cells (at  $10^6 \text{ cells ml}^{-1}$ ) was calculated over 3 h (Methods), for the same three bacterial phenotypes (WT,  $\Delta cheA$  and  $\Delta fliC$ ) used in the experiments. Results revealed an increased uptake of DOM by WT cells compared with both  $\Delta cheA$  and  $\Delta fliC$  mutants (Extended Data Fig. 2), in agreement with experimental results (Fig. 2b). Specifically, chemotactic cells (WT) exhibited a 2.1-, 1.3- and 1.1-fold increase in DOM uptake over the  $\Delta cheA$  mutants, for *Synechococcus* concentrations of  $10^3$ ,  $10^4$  and  $10^5 \text{ cells ml}^{-1}$ , respectively.

Investigation of individual bacterial trajectories from the mathematical model revealed the fleeting nature of the interactions between bacteria and picophytoplankton. We defined the phycosphere radius,  $R_p = 35 \mu\text{m}$ , as the distance from individual *Synechococcus* cells at which the bacterial chemotactic response was strongest (Methods and Extended Data Fig. 3). This allowed us to quantify from the model the residence time  $\tau$  associated with each encounter of a bacterium with a *Synechococcus* phycosphere (Fig. 3), defined as the time between entry to and departure from the phycosphere (Fig. 3a). Computing the residence time for all bacteria–phycosphere encounters revealed that WT cells spend on average three times longer in *Synechococcus* phycospheres ( $\tau = 3.2 \pm 11.5 \text{ s}$ ,  $n = 82,242$  encounters) than  $\Delta cheA$

mutants ( $\tau = 1.0 \pm 1.4 \text{ s}$ ,  $n = 2,626$  encounters; Fig. 3b,c). The difference was even more pronounced for longer encounters, with residence times greater than 10 s being 16 times more likely for WT cells (7.3% of encounters) than for  $\Delta cheA$  mutants (0.46% of encounters).

Beyond the duration of individual encounters, our trajectory analysis revealed that chemotaxis strongly affects the number of unique phycosphere encounters per day. At a *Synechococcus* concentration of  $10^3 \text{ cells ml}^{-1}$ , chemotaxis more than tripled the mean encounter rate of bacteria with phycospheres (WT:  $12.6 \text{ day}^{-1}$ ;  $\Delta cheA$ :  $4.1 \text{ day}^{-1}$ ; Fig. 3d). The distribution of encounters revealed that 29% of WT cells but only 0.7% of  $\Delta cheA$  cells encountered more than 15 unique phycospheres per day. Moreover, the top 5% of WT cells encountered on average 36 unique phycospheres per day, compared with only 13 for the top 5% of  $\Delta cheA$  cells (Fig. 3d).

The phycosphere afforded WT bacteria a substantial fraction of their uptake, even though time spent in the phycosphere was short. Our model revealed that WT bacteria derived 30% of their total DOM uptake from the phycosphere, despite spending merely 1.7% of time in it. In stark contrast, for  $\Delta cheA$  bacteria, the proportion of DOM uptake originating from the phycosphere was ~100-fold smaller—they derived just 0.38% of their DOM uptake from the phycosphere, where they spent only 0.02% of time. We conclude that the differences in residence time, coupled with the sharp spatial decay of the DOM concentration in the phycosphere (Extended Data Fig. 4), is the cause of the significant enhancement in DOM uptake conferred by chemotaxis.

### Chemotaxis provides growth advantages

To further explore how chemotactic behaviour may affect the fitness of heterotrophic bacteria, we conducted a multi-day co-culture experiment between *Synechococcus* and each of the three *M. adhaerens* phenotypes (at a starting concentration of  $10^3 \text{ cells ml}^{-1}$  for both partners). Our results demonstrate that WT *M. adhaerens* grew significantly

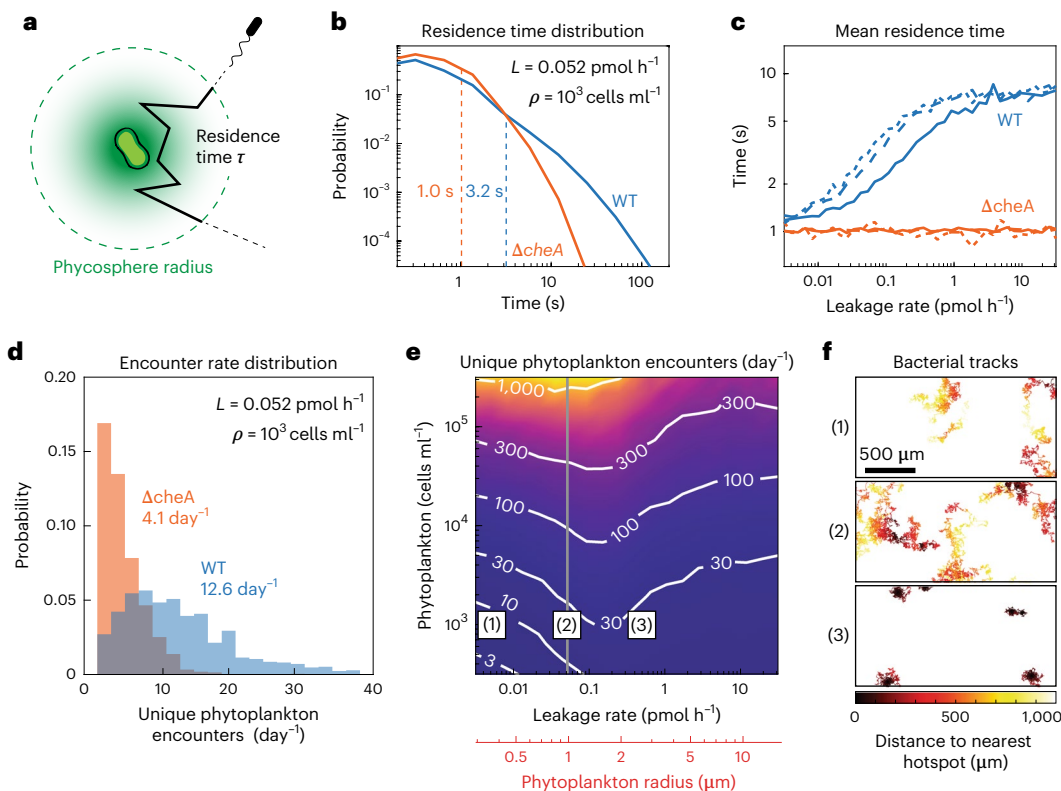


**Fig. 3 | Numerical simulations reveal the dynamic interactions between *Marinobacter* and *Synechococcus*.** **a,b**, The duration of every bacterium–phytoplankton interaction (residence time  $\tau$ ) was recorded throughout the simulations (a), revealing that WT *M. adhaerens* cells spend, on average, more than three times longer within each phycosphere ( $R_p = 35 \mu\text{m}$ ) than chemotaxis-deficient mutants (WT:  $3.2 \pm 1.5 \text{ s}$ ;  $\Delta\text{cheA}$ :  $1.0 \pm 1.4 \text{ s}$ ) (b). For WT cells, 0.58% of encounters were for more than 60 s, while the longest residence time for  $\Delta\text{cheA}$  cells was 23 s ( $n = 2,626$  encounters). **c**, Mean residence time as a function of leakage rate  $L$  (or the equivalent effective phytoplankton radius) for three

*Synechococcus* concentrations ( $10^3 \text{ cells ml}^{-1}$ : dotted,  $10^4 \text{ cells ml}^{-1}$ : dashed, and  $10^5 \text{ cells ml}^{-1}$ : solid). **d**, The number of unique phytoplankton encounter per day depended strongly on the bacterial motility strategy (mean WT:  $12.6 \text{ day}^{-1}$ ;  $\Delta\text{cheA}$ :  $4.1 \text{ day}^{-1}$ ). **e**, The mean rate of unique phytoplankton encounters as a function of phytoplankton leakage rate and cell concentration for the WT simulations. **f**, Bacterial trajectories for three different phytoplankton radii, (1)  $R = 0.36 \mu\text{m}$  ( $L = 0.1L_0$ ), (2)  $R = 1 \mu\text{m}$  ( $L = L_0$ ) and (3)  $R = 2.7 \mu\text{m}$  ( $L = 10L_0$ ), where  $L_0$  is the value for *Synechococcus*. Bacterial trajectories are colour coded on the basis of the instantaneous distance to the nearest phytoplankton cell.

faster in co-culture with *Synechococcus* than the non-motile mutant and the non-chemotactic mutant (repeated-measure ANOVA,  $P < 0.05$ ; Supplementary Table 9 and Extended Data Fig. 5). This effect was sustained over 4 days while *Synechococcus* concentrations remained low, but disappeared as *Synechococcus* increased in abundance beyond  $10^5 \text{ cells ml}^{-1}$  (Extended Data Fig. 5). Importantly, this growth enhancement occurred despite both  $\Delta\text{cheA}$  and  $\Delta\text{flfC}$  mutants growing significantly faster than the WT under nutrient-replete conditions (repeated-measure ANOVA,  $P < 0.05$ ; Supplementary Table 10 and Extended Data Fig. 5). These results reveal that the greater nutrient uptake achieved by chemotactic cells over short timescales (minutes to hours) ultimately increases cell fitness over longer timescales (days).

Our numerical simulations allowed us to extend the analysis to phytoplankton cells of different sizes, and explore the relative advantage provided by chemotaxis across a range of realistic nutrient sources (Fig. 4). Indeed, our simulations revealed that the advantage of chemotaxis is most pronounced at low phytoplankton concentrations, regardless of the phytoplankton cell sizes (or equivalently nutrient leakage rate). However, the relative advantage provided by chemotaxis increased with phytoplankton size, with a >50-fold enhancement in DOM exposure over  $\Delta\text{cheA}$  mutants when interacting with large but widely separated phytoplankton (Fig. 4). In addition, larger phytoplankton sizes dramatically increase the mean residence time of chemotactic bacteria (Fig. 3c), ultimately suppressing the transient interactions reported for *Synechococcus* and limiting bacterial dispersal (Fig. 3e,f). These data

indicate qualitatively distinct bacterial interactions with small and large phytoplankton, respectively, and can serve as a blueprint for studying ecological interactions in different regimes.

Our experiments were carried out in laboratory conditions whereby cells were suspended in a nitrogen- and phosphorous-rich medium, which is not directly reflective of the nutrient-limiting conditions prevailing in the oligotrophic ocean, and this could potentially influence rates of exudation by *Synechococcus* cells. The factors governing the exudation rates of organic substrates from phytoplankton cells are still largely unresolved<sup>12</sup>, and ambient nutrient levels may potentially influence exudation rates. While some evidence suggests that exudation rates are enhanced in oligotrophic conditions<sup>33</sup>, it is also possible that under nutrient-limited conditions *Synechococcus* cells may reduce the amount of nitrogen they exude. This uncertainty notwithstanding, our numerical simulations indicate that, even if the leakage rate of *Synechococcus* cells was substantially smaller than the one observed in our experiments (that is,  $L = 0.01 \text{ pmol h}^{-1}$ ), the relative enhancement in nutrient exposure due to chemotaxis would still be sizeable (for example, 11% enhancement if the exudation rate was five times smaller; Fig. 4).

## Discussion

The principal goal of our study was to determine whether chemotaxis enhances heterotrophic bacterial exposure to, and assimilation of, substrates released into the phycosphere of picophytoplankton.

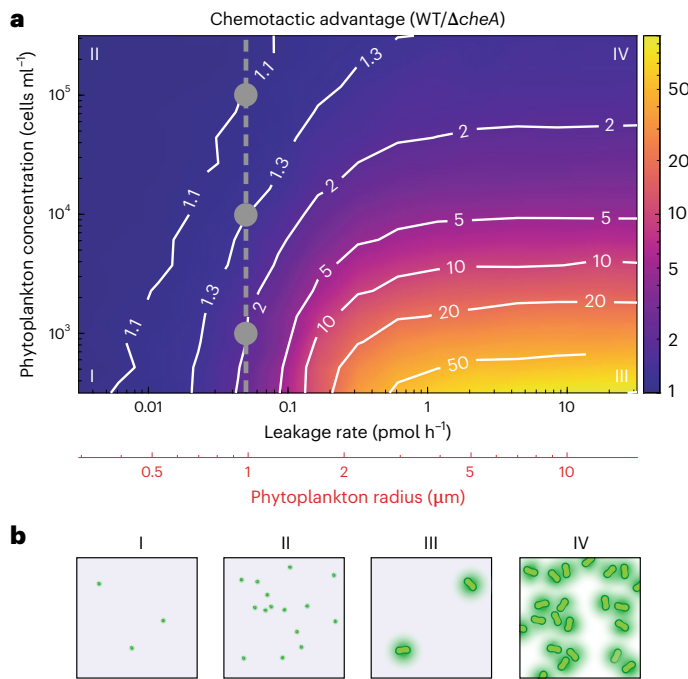


**Fig. 4 | DOM enhancement due to chemotaxis depends strongly on the size and concentration of phytoplankton cells.** **a**, The relative DOM exposure (ratio) for chemotactic bacteria (WT) compared with non-chemotactic mutants ( $\Delta cheA$ ) as a function of the effective phytoplankton size (controlled through the leakage rate,  $L$ ), and phytoplankton concentration. Grey circles correspond to the experimental treatments in Figs. 1 and 2. Roman numeral placement in the parameter space corresponds to image panels. **b**, Schematic representation of phytoplankton sizes and densities depicted by the Roman numerals in **a**.

Motility comes at an energetic cost for cells<sup>34</sup>, which we have not explicitly considered here. This energetic cost would partly offset the nutrient uptake advantage and could result in there being a *Synechococcus* cell concentration below which motility no longer provides an advantage. In our experiments, no significant difference in <sup>15</sup>N uptake between non-chemotactic and non-motile cells was recorded over short co-incubations (Fig. 2b), suggesting that the energetic cost of swimming was not detectable over that timeframe (3 h). However, during longer co-incubations (12 days), the non-motile cells grew on average 24.5% faster than the non-chemotactic ones (Extended Data Fig. 5), potentially due to the cost of building and operating the flagellar apparatus.

Taken together, our experimental and modelling results (1) provide the first quantitative demonstration that chemotaxis enhances the uptake of phytoplankton-derived metabolites by motile heterotrophic marine bacteria and (2) overturn the paradigm (previously based on the chemotactic parameters from *E. coli*<sup>22</sup>) that marine bacteria will not be able to use chemotaxis towards individual picophytoplankton. The latter points to a greater chemotactic sensitivity of marine bacteria compared with *E. coli*, which is in line with prior observations on the chemotaxis of marine bacteria<sup>32,35</sup>. Picophytoplankton collectively amount to a biomass similar to diatoms at the global scale (12.7 and 16.5  $\mu\text{g C l}^{-1}$ , respectively)<sup>36</sup>, despite their diameter being 10–100-fold smaller<sup>36</sup>, and are the dominant phototrophic organisms in many parts of the oligotrophic ocean<sup>17</sup>. Our findings therefore expand the potential for chemotaxis to govern the ecological and metabolic interactions between heterotrophic bacteria and phytoplankton to a major fraction of phototrophic biomass in the ocean.

Our results show that chemotactic bacteria benefit from phytoplankton not just by migrating into and retaining position within

their phycosphere, as occurs for larger phytoplankton<sup>16</sup>, but through transient spatial associations with the phycospheres. These brief encounters still provide conspicuous advantages, because spending even a small fraction of time in the highly DOM-enriched vicinity of phytoplankton cells translates into large increases in DOM uptake<sup>16</sup>. Given the abundance of picophytoplankton in the global ocean<sup>17</sup>, these fleeting interactions will be numerous, providing a viable strategy for nutrient exchanges in the water column. Rather than stably associating with *Synechococcus*, chemotactic heterotrophs therefore derive a competitive advantage over their non-chemotactic counterparts because they can considerably extend the frequency and duration of their spatial association with picophytoplankton, even if each encounter is highly transient.

Our experiments reveal that these transient interactions increase not only the uptake of *Synechococcus*-derived dissolved organic nitrogen by heterotrophs, but also the uptake of heterotroph-derived carbon by *Synechococcus* cells. This indicates that chemotactic behaviour can foster reciprocal metabolic exchange between marine microorganisms and thereby potentially enhance primary and secondary production levels and rates of nutrient recycling, even in the large regions of ocean dominated by small phytoplankton cells. Chemotaxis is recognized as a pervasively important behaviour enabling the onset and maintenance of symbiotic interactions across different hosts and environments<sup>34</sup>; however, symbiosis commonly refers to spatially close and temporally extended interactions between organisms<sup>37</sup>. Although very different from this traditional view, the short-lived yet repeated encounters described here benefit both partners and may contribute to their survival in the resource-poor open ocean. These partnerships might therefore represent ‘transient’ symbioses, at the opposite end of obligate intracellular associations on the symbiotic continuum. Taken together, these observations suggest that, even across the large areas of the ocean where phototrophic biomass is dominated by very small cells, sophisticated metabolic interactions among the plankton, facilitated by microbial foraging behaviours, can influence oceanic productivity and biogeochemical cycling. Furthermore, our quantification of the benefits of chemotactic interactions between very small cells highlights that chemotaxis may play an unexpected role in the metabolic exchanges between individual bacterial cells across all environments.

## Methods

### Cultures

*Synechococcus* sp. CS-94 RRIMP N1 (ref. <sup>38</sup>) was grown in enriched seawater, artificial water (ESAW)<sup>39</sup> complemented with f/2 nutrients<sup>40</sup>. The cells were maintained at 23 °C on a 12:12 h dark:light cycle at ~180  $\mu\text{mol photons m}^{-2} \text{s}^{-1}$ . In addition, we used the WT marine bacterium *M. adhaerens* HP15 (ref. <sup>41</sup>) (motile and chemotactic),  $\Delta cheA$ , a motile but non-chemotactic mutant<sup>13</sup>, and  $\Delta fliC$ , a non-motile mutant<sup>42</sup>. In  $\Delta cheA$  or  $\Delta fliC$  mutants, the genes *cheA* or *fliC*, respectively, were replaced by a chloramphenicol resistance cassette using homologous recombination on the up- and downstream regions of the genes, as described previously<sup>13,42</sup>. Both mutants were complemented with medium-copy number plasmids (pBBR1MCs-based) containing *cheA* or *fliC*, downstream of the *lac* promoter of the vector. This was needed since neither of these two genes carries their own promoter. These complemented mutants were tested in the respective assays with tenfold-diluted MB 0.3% soft agar (for *cheA* mutant transformant) and the MB 0.3% soft agar assay (*fliC* mutant transformant), showing restoration of WT levels of motility.

To determine the growth dynamics of the three *M. adhaerens* HP15 phenotypes (WT,  $\Delta cheA$  and  $\Delta fliC$ ), single colonies were picked from Marine Agar plates (Difco Laboratories) and resuspended in Marine Broth (Difco Laboratories). Cell concentrations were quantified using flow cytometry (CytoFLEX S, using CytExpert Version 2.4, Beckman Coulter), using filtered MilliQ water as the sheath fluid and a flow rate

of  $25 \mu\text{l min}^{-1}$ . Cells were fixed with glutaraldehyde (final concentration 2%) and then stained with SYBR Green (final concentration 1:10,000) for 15 min in the dark<sup>43</sup>. For each sample, forward scatter (FSC), side scatter (SSC), green (488 nm, SYBR) and red (650 nm) fluorescence were recorded. *Marinobacter* cells were characterized according to SSC and SYBR Green fluorescence<sup>43</sup>. Flow cytometric counts were used to normalize the starting concentration of *Marinobacter* cells (WT,  $\Delta cheA$  and  $\Delta fliC$ ,  $n = 3$  for each treatment) to 10,000 cells  $\text{ml}^{-1}$  in Marine Broth (Difco Laboratories). Cells were incubated at 23 °C with shaking (180 r.p.m.), and 100  $\mu\text{l}$  was sampled every two hours from each culture. Cells were then immediately fixed with glutaraldehyde and enumerated as outlined above. To enumerate cell concentrations in each treatment over a 24 h period, triplicate starting cultures for each treatment were set up twice 12 h apart. The first set of cultures was enumerated for the first 10 h, and 12 h later, the second set of cultures was enumerated between 10 h and 24 h.

### Isotope labelling

To quantify the reciprocal exchanges of nutrients between *Synechococcus* and *M. adhaerens*, the cells were pre-labelled with the stable isotopes  $^{15}\text{N}$  and  $^{13}\text{C}$ , respectively. *Synechococcus* cells were inoculated into ESAW complemented with f/2 with  $^{15}\text{N}$ -labelled sodium nitrate ( $\text{NaNO}_3$ ,  $^{15}\text{N}$ , 98%+, Cambridge Isotopes Laboratories) as sole source of nitrogen (0.882 mM; same concentration as f/2). The cells were grown in 50 ml for 1 week, under the same conditions as above, to ensure high level of  $^{15}\text{N}$  enrichment in the cells. Two days before the experiment, glycerol stocks of the three *M. adhaerens* phenotypes were streaked onto respective Difco 2216 Marine Agar plates (Difco Laboratories) and incubated at 30 °C. The day before the experiment, single colonies of each of the *Marinobacter* phenotypes were suspended into ESAW medium enriched with  $^{13}\text{C}$ -labelled amino-acids (1 g  $\text{l}^{-1}$  Cetone Base Powder; 98%+  $^{13}\text{C}$ , Cambridge Isotope Laboratories) and grown for 12 h at 30 °C with shaking (180 r.p.m.), to ensure that the three *Marinobacter* phenotypes were in the same growth phase before the start of the experiment. Note: *M. adhaerens* HP15 lacks all genes required for dissimilatory or assimilatory nitrate reduction based on its genome annotation (<https://www.genome.jp/entry/gn:T01922>).

### Experimental conditions

On the day of the experiment, both *Synechococcus* and *M. adhaerens* cells were rinsed three times to remove all residual stable isotopes from their respective media. Specifically, *Synechococcus* cells were centrifuged at 1,500g for 15 min, and the supernatant was discarded and replaced with fresh f/2 medium containing natural abundances of  $^{15}\text{N}$ . These washing steps were performed three times before resuspending the cells in 50 ml of f/2. These repeated medium exchanges (from  $^{15}\text{N}$  enriched f/2 to natural abundance) were carried out to ensure that no enriched level of  $^{15}\text{NaNO}_3$  was present in the growth medium when the co-incubation started. The same washing procedure was applied to the overnight *Marinobacter* cultures to remove  $^{13}\text{C}$  from the medium before inoculation.

The cell concentrations of both *Synechococcus* and the three *Marinobacter* phenotypes were then determined by flow cytometry (CytoFLEX S, Beckman Coulter), using filtered MilliQ water as the sheath fluid and a flow rate of  $25 \mu\text{l min}^{-1}$ . Cells were fixed with glutaraldehyde (final concentration 2%) for 15 min. Before analysis, the *Marinobacter* samples were stained with SYBR Green (final concentration 1:10,000) for 15 min in the dark<sup>43</sup>. For each sample, FSC, SSC, green (488 nm, SYBR) and red (650 nm) fluorescence were recorded (Supplementary Fig. 1). *Marinobacter* cells were characterized according to SSC and SYBR Green fluorescence<sup>43</sup>, while *Synechococcus* were discriminated according to SSC and red fluorescence (through the autofluorescence of photosynthetic pigments). Cell counts were used to adjust the *Synechococcus* densities to three discrete concentrations: 1,000, 10,000 and 100,000 cells  $\text{ml}^{-1}$ . Each of the three strains of

*M. adhaerens* was inoculated separately at a final concentration of  $10^6$  cells  $\text{ml}^{-1}$  in each *Synechococcus* cell density.

*Synechococcus* and *M. adhaerens* strains were co-incubated in triplicates for 3 h (based on pilot studies), during the light cycle, under the same light and temperature conditions used for maintaining *Synechococcus*. At the end of the experiment, samples were fixed with glutaraldehyde (final concentration 2%) for 30 min. A *Synechococcus* culture maintained in natural abundance of  $^{15}\text{N}$  and a *M. adhaerens* culture maintained in natural abundance of  $^{13}\text{C}$  were used as unlabelled controls; these cells were treated identically to all other experimental cultures. To remove any residual glutaraldehyde, the samples were washed with ESAW after pelleting the cells by centrifugation (1,500g for 15 min). Finally, the cells were resuspended in 50  $\mu\text{l}$  of sterile filtered MilliQ water (to remove ESAW salts) and the full volume was immediately placed onto silicon wafers (7.07 mm × 7.07 mm, Type P/<111>, ProSciTech), dried at 45 °C and stored inside a desiccator, protected from light until NanoSIMS analysis. Finally, the samples were coated with 5 nm of gold before being loaded in the NanoSIMS.

### NanoSIMS analysis

We used the NanoSIMS 50 (CAMECA) at the Centre for Microscopy, Characterisation and Analysis (CMCA) at The University of Western Australia. This instrument allows for simultaneous collection of up to five isotopic species (here:  $^{12}\text{C}_2^-$ ,  $^{12}\text{C}^{13}\text{C}^-$ ,  $^{12}\text{C}^{14}\text{N}^-$ ,  $^{12}\text{C}^{15}\text{N}^-$  and  $^{32}\text{S}$ ). Enrichment of the rare isotopes  $^{15}\text{N}$  and  $^{13}\text{C}$  was confirmed by an increase in the  $^{15}\text{N}/^{14}\text{N}$  or  $^{13}\text{C}/^{12}\text{C}$  ratio above the natural abundance value recorded in the control (equal to  $0.003716 \pm 0.000005$  for nitrogen in *Marinobacter* cells and  $0.011167 \pm 0.000027$  for carbon in *Synechococcus* cells). The NanoSIMS was performed using a chain analysis: samples were pre-sputtered for 3.5 min at 500 pA  $\text{Cs}^+$  beam ( $D_1 = 1$ ) on  $30 \mu\text{m}^2$  areas ( $256 \times 256$  pixel), followed by automatic horizontal and vertical secondary ion beam centring. The analysis was then performed by rastering a 2 pA beam ( $D_1 = 2$ ) over  $25 \mu\text{m}^2$  areas ( $256 \times 256$  pixels); three planes were recorded per area with a dwell time of 3 ms per pixel. The instrument was operated with a high mass resolving power (in the range of 9,000), allowing the separation of isobaric interferences, and was calibrated daily using yeast cells harbouring natural abundance of C, N and S. Images were analysed using the Fiji software package (version 1.53c) (<http://fiji.sc/Fiji>)<sup>44</sup> combined with the OpenMIMS plug-in (<http://nrims.harvard.edu/software>). All images were dead-time corrected<sup>45</sup>, and the individual planes were then summed before extracting counts from the images. Isotopic quantification data were extracted from the mass images by manually drawing regions of interest around each bacterial cell using the  $^{12}\text{C}^{14}\text{N}^-$  image as mask. No cell attachment was observed between the two bacterial species in any of the experiments.

### Calculation of net fixation (uptake)

We converted our NanoSIMS data into percentage of C or N incorporated into the microorganism relative to the initial C or N content, respectively. This net fixation ( $F_{X_{\text{net}}}$ ) (ref. <sup>46</sup>) is equal to:

$$F_{X_{\text{net}}} = \frac{R_f \left( 1 - \frac{R_i}{R_i + 1} \right) - \frac{R_i}{R_i + 1}}{\frac{R_s}{R_s + 1} - R_f \left( \frac{1}{R_s + 1} \right)} \times 100 \quad (1)$$

where  $R_i$  is the initial isotopic ratios of the organism prior,  $R_f$  the final isotopic ratio of the sampled organism and  $R_s$  the isotopic ratios in the pre-enriched partner organism.

### Characterization of *Synechococcus* and *M. adhaerens* HP15 WT metabolites

A 2-litre *Synechococcus* culture was grown for 1 week in ESAW supplemented with f/2 nutrients as described above. A 2-litre *M. adhaerens* culture (WT) was grown overnight as described above (10% Cetone Base Powder in ESAW; Cambridge Isotope Laboratories). To characterize the

cell exudates, cells were pelleted at 1,500g for 15 min and resuspended individually in fresh ESAW supplemented with f/2 nutrients for 3 h. Following this incubation, cells were pelleted at 1,500g for 15 min and the supernatant was filtered through a 0.45 µm filter, and then through a 0.2 µm filter to ensure the removal of all cells. The filtrate was acidified to pH 2 using 10% HCl (made with HPLC water from HCl puriss. 32%, Fluka, Sigma), spiked with internal standards (0.5% final concentration;  $^{13}\text{C}_6$ -sorbitol;  $^{13}\text{C}$ - $^{15}\text{N}$ -valine, penta-fluorobenzoic acid and 2-aminoanthracene) and subjected to a solid phase extraction (12 cc, 500 mg sorbent; HLB cartridges, Oasis). After the complete elution of the filtrate, the solid phase extraction cartridges were washed twice with 6 ml of 0.01 N HCl to remove residual salts and dried for 20 min under vacuum. Finally, the metabolites were eluted with 4 ml of HPLC-grade methanol (Sigma-Aldrich) into glass vials and stored at -20 °C until needed.

### Metabolomics: sample derivatization

Dried samples for targeted analysis were prepared by adding 25 µl of methoxyamine hydrochloride (30 mg ml<sup>-1</sup> in pyridine) followed by shaking at 37 °C for 2 h. Samples were then derivatized with 25 µl of *N,O*-bis(trimethylsilyl)trifluoroacetamide with trimethylchlorosilane (BSTFA with 1% TMCS, Thermo Scientific) for 1 h at 37 °C. Samples were left for 1 h before 1 µl was injected onto the gas chromatography column using a hot needle technique. Split (1:10) injections were done for each sample.

### Metabolomics: analytical instrumentation

The GC-MS system used was composed of an AOC6000 autosampler, a 2030 Shimadzu gas chromatograph and a TQ8050 quadrupole mass spectrometer (Shimadzu). The mass spectrometer was tuned according to the manufacturer's recommendations using tris-(perfluorobutyl)-amine (CF43). GC-MS was performed on a 30 m Agilent DB-5 column with 1 µm film thickness and 0.25 mm internal diameter column. The injection temperature (inlet) was set at 280 °C, the MS transfer line at 280 °C and the ion source adjusted to 200 °C. Helium was used as the carrier gas at a flow rate of 1 ml min<sup>-1</sup>, and argon gas was used as the collision cell gas to generate the multiple reaction monitoring (MRM) product ion. Sample analysis was performed under the following temperature programme; start at injection 100 °C, a hold for 4 min, followed by a 10 °C min<sup>-1</sup> oven temperature ramp to 320 °C following final hold-off for 11 min. Approximately 520 quantifying MRM targets were collected using Shimadzu Smart Database along with qualifier for each target that covers about 350 endogenous metabolites and multiple  $^{13}\text{C}$ -labelled internal standards. Both chromatograms and MRMs were evaluated using the Shimadzu GC-MS browser and LabSolutions Insight software. This approach is classified as level 1-2 (ref. <sup>47</sup>) or level C according to the proposed reporting standards by the Metabolite Identification Task Group of the Metabolomics Society (<http://metabolomicssociety.org/board/scientific-task-groups/metabolite-identification-task-group>). Resulting area responses were normalized to the internal standard  $^{13}\text{C}_6$ -sorbitol area response.

### Chemotaxis assay

To test the chemotactic response of *M. adhaerens* HP15 (WT) towards *Synechococcus* metabolites, we performed a chemotaxis assay using the In Situ Chemotaxis Assay (ISCA)<sup>30</sup>. The ISCA is a microfluidic device composed of an array of microwells that can be filled with different chemoattractants. Here we used: (1) ESAW as negative control, (2) *Synechococcus* exudates (generated for metabolite analysis above; 1 mg ml<sup>-1</sup>) and (3) 10% Marine Broth (BD Difco) as positive control. Each chemical was resuspended in ESAW and filtered (0.2 µm).

*M. adhaerens* HP15 (WT) cells were grown on plate for 3 days. Colonies were then transferred into 0.22-µm-filtered ESAW (room temperature). *M. adhaerens* cells numbers were then adjusted to 10<sup>6</sup> cells ml<sup>-1</sup> with 0.22-µm-filtered ESAW. Each ISCA ( $n = 5$ ) was

deployed in the *M. adhaerens* suspension (80 ml) for 30 min (ref. <sup>48</sup>). At the end of the incubation, ISCA well contents were collected and fixed with glutaraldehyde (2% final concentration) for 15 min. Cell abundance in each ISCA treatment ( $n = 5$ ) was quantified by running a standardized volume of sample (50 µl) by flow cytometry as described above. To quantify the strength of chemotaxis, the chemotactic index (*Ic*) was calculated by dividing the number of cells present in each treatment by the number of cells present in the filtered seawater control<sup>30</sup>.

### Co-growth experiments

Co-cultures were established between each of the three *Marinobacter* phenotypes (WT,  $\Delta\text{cheA}$  and  $\Delta\text{flfC}$ ) and *Synechococcus*. *Marinobacter* were grown on Marine Agar plates (Difco Laboratories) for 3 days, single colonies were transferred into Marine Broth and grown overnight (12 h). Cells were washed with sterile f/2 medium and diluted 1:100 in f/2. A 200 µl aliquot was fixed with glutaraldehyde and stained with SYBR Green for enumeration via flow cytometry as described above. *Synechococcus* from a 7 day culture were also diluted 1:100 in f/2 and enumerated using flow cytometry as described above. Co-cultures were then set up by inoculating both *Synechococcus* and *Marinobacter* into fresh f/2 medium at a standardized cell density of ~1,000 cells ml<sup>-1</sup> ( $n = 4$ ). Co-cultures were incubated at 23 °C on a 12:12 h dark:light cycle at ~180 µmol photons m<sup>-2</sup> s<sup>-1</sup> and shaken every 4 h (180 r.p.m. for 15 min) to keep cells in suspension. Cell densities were then enumerated every day for 12 days using flow cytometry as described above.

### Statistical analysis

Growth data were analysed using repeated-measure ANOVA after assessing the normality and sphericity of the data. Simple main effect tests were then used to assess whether treatments were significantly different at each timepoint (*P* values were corrected using Bonferroni). The chemotaxis responses of *Marinobacter* were then analysed using a one-way ANOVA. As the NanoSIMS data were not normally distributed and/or not homogeneous, KW test, followed with pairwise Wilcoxon tests, was carried out to test the  $^{15}\text{N}$  and  $^{13}\text{C}$  of the target cells. All *P* values were corrected using the Benjamini–Hochberg procedure for multiple comparisons. All statistical analyses were carried out in R v4.1.1 (ref. <sup>49</sup>), and analysis scripts are available on GitHub (<https://github.com/JB-Raina-codes/Synechococcus-paper>).

### Mathematical model for bacteria–phytoplankton interactions

**Modelling chemical microenvironments of *Synechococcus*.** To model the DOM landscape, individual *Synechococcus* cells were considered as point-wise particles, exuding DOM at a rate *L* (molecules per unit time). We begin by considering the DOM concentration around a single *Synechococcus* cell in an unbounded, quiescent fluid. The exuded molecules diffuse radially and are consumed by bacteria distributed throughout the domain. Owing to the spherical symmetry of the problem, both the DOM concentration, *C*(*r*, *t*), and the bacterial concentration, *B*(*r*, *t*), may be written as functions of distance, *r*, from the *Synechococcus* cell, and time, *t*. The DOM profile varies in space and time according to the diffusion equation<sup>16</sup>:

$$\frac{\partial C}{\partial t} = D\nabla^2 C - [4\pi aDB(r, t)]C. \quad (2)$$

The first and second terms on the right-hand side of equation (2) represent the molecular diffusion of DOM and the diffusion-limited uptake by bacteria, respectively. Amino acids constitute a large fraction of the *Synechococcus* exudates (Supplementary Table 2), and given their similar respective molecular weights, we represent the exudate as a single molecular species. Glutamate was chosen (diffusivity *D* = 608 µm<sup>2</sup> s<sup>-1</sup>), since its capacity to elicit chemotaxis is well studied<sup>32</sup>. The second term on the right-hand side of equation (2) represents diffusion-limited consumption of the DOM source by bacteria. The

parameter  $a$  is the cell radius of *M. adhaerens*. The distribution of bacteria,  $B(r, t)$ , will in general not be uniform, and will depend on  $C(r, t)$ . However, if we assume that bacteria are approximately uniformly distributed with concentration  $B_0$ , equation (2) may be rewritten as:

$$\frac{\partial C}{\partial t} = D\nabla^2 C - kC, \quad (3)$$

where the diffusion-limited consumption rate is given by  $k = 4\pi a DB_0$ . The steady-state solution to equation (3) in spherical coordinates, which is finite at  $r \rightarrow \infty$ , is given by

$$C(r) = \frac{A}{r} \exp\left(-\sqrt{\frac{k}{D}}r\right) = \frac{A}{r} \exp(-\sqrt{4\pi a B_0} r), \quad (4)$$

where  $A > 0$  is an arbitrary constant. The radial flux of DOM through a spherical surface at  $r = \epsilon \ll 1$  must match the leakage rate from the *Synechococcus* cell. That is,

$$\lim_{r \rightarrow 0} \left( -D \frac{dC}{dr} 4\pi r^2 \right) = 4\pi AD = L. \quad (5)$$

It follows that

$$C(r) = \frac{L}{4\pi Dr} \exp(-\sqrt{4\pi a B_0} r). \quad (6)$$

Note that the above expression diverges at  $r \rightarrow 0$ . However, for any bacterium in the vicinity of the DOM source, the maximum concentration of DOM it may experience occurs at the surface of *Synechococcus* (with radius  $r_0 = 1 \mu\text{m}$ ). The DOM profile is therefore capped by this value, so that

$$C(r) = \begin{cases} \frac{L}{4\pi D r_0} \exp(-\sqrt{4\pi a B_0} r_0), & r \leq r_0 \\ \frac{L}{4\pi D r} \exp(-\sqrt{4\pi a B_0} r), & r > r_0 \end{cases} \quad (7)$$

We note that the total amount of DOM present in the domain,  $\int C(r) dV$ , is finite, as the phytoplankton leakage is balanced by bacterial consumption. It is possible to recover the DOM profile in the absence of bacterial consumption by setting  $B_0 = 0$ . The resulting functional form,  $C(r) = L/4\pi Dr$ , is used elsewhere<sup>12</sup> in the case of single hotspots. However, for a suspension of *Synechococcus* cells, the long-range nature of this function results in a divergent DOM concentration. It is therefore necessary to utilize the more realistic profile shown in equation (7), which encompasses the effect of bacterial consumption. For the purposes of calculating the DOM profile in equation (7), the experimental value of  $B_0 = 10^6 \text{ cells ml}^{-1}$  is used.

The DOM profile presented in equation (6) assumes an infinite bacterial suspension surrounding an individual *Synechococcus* cell. We explicitly examine the role that diffusion-limited uptake has in shaping the DOM profile (Extended Data Fig. 4a). For four different bacterial concentrations,  $B_0$  ( $\text{cells ml}^{-1}$ ), the DOM profile is shown. Dilutions by factor 2 and 5 from the experimental concentration of  $B_0 = 10^6 \text{ cells ml}^{-1}$  only slightly affect the resultant DOM profile.

We also test the effect of truncating bacterial density beyond a critical radius, so that  $B = B_0$  for  $r < R_0$  and  $B = 0$  beyond this radius. This is essential for assessing the role of interacting phycospheres, where the background concentration of bacteria would not necessarily exhibit the same diffusion-limited uptake for multiple patches simultaneously. Extended Data Fig. 4b shows the exact solution to equation (2) with a step change in bacterial concentration outlined above. Both the dark-green curve (bacteria everywhere:  $R_0 = \infty$ ) and black curve (no bacteria:  $R_0 = 0$ ) are identical to those presented in panel A. Truncating the bacterial concentration to lie only in  $R_0 < 1,000 \mu\text{m}$  and  $R_0 < 500 \mu\text{m}$

barely modifies the DOM concentration profile. In other words, the uptake of DOM by bacteria in the far field is not important for regulating the DOM profile in the vicinity of the phytoplankton cell. As a result, we are able to directly apply equation (6) for a 3D suspension of multiple *Synechococcus* cells.

**Model for multiple resources.** To mimic the experimental system, we considered a rectangular box with dimensions  $l_x = l_y = l_z = l$  in the  $x, y, z$  directions respectively. This box is seeded with  $N$  identical DOM sources at random positions in space  $\{\mathbf{x}_i = (x_i, y_i, z_i) | i = 1, 2, \dots, N\}$  so that the total concentration of *Synechococcus* cells is  $\rho = N/l^3$ . In all simulations conducted, we set  $N = 250$ , and vary  $\rho$  by changing the dimensions of the box,  $l$ . Linearity of the diffusion equation enables the superposition of multiple solutions from equation (7). It follows that the total DOM concentration at position  $\mathbf{x}$  is given by

$$C(\mathbf{x}) = \sum_{i=1}^N C_i(d_i), \quad (8)$$

where  $C_i$  is the expression in equation (7) and  $d_i$  is the distance between points  $\mathbf{x}$  and  $\mathbf{x}_i$ . We utilize periodic boundary conditions to evaluate  $d_i$ , so that the concentration resulting from each *Synechococcus* cell is evaluated by taking the shortest distance to it within the periodic domain. From equations (7) and (8), it is also possible to directly evaluate the spatial gradient of the DOM field, given by  $\nabla C(\mathbf{x})$ . A single 2D slice of the DOM profile through the box domain with *Synechococcus* concentration  $\rho = 10^3 \text{ cells ml}^{-1}$  is shown in Extended Data Fig. 6.

**Model for bacterial chemotaxis.** We introduce bacteria into the three-dimensional DOM field defined by equation (8) and investigate their collective dynamics. The relative performance (DOM exposure) of WT bacteria compared with their non-chemotactic or non-motile counterparts is examined. To begin with, we outline the agent-based model for bacterial chemotaxis. This model incorporates the essential features of bacterial navigation, and accurately captures the chemotaxis of another marine bacterium, *Vibrio ordalii*<sup>32</sup> responding to dissolved glutamate sources (less than 1% fitting error). Where possible, we have updated specific model parameters for the case of *M. adhaerens* (for all model parameters, see Supplementary Table 8).

In the laboratory frame, the DOM concentration is given by the smooth function  $C(\mathbf{x})$ . In each simulation timestep,  $\Delta t = 0.10 \text{ s}$ , a bacterium with velocity  $\mathbf{v}$  and position  $\mathbf{x}$  performs a noisy measurement of the concentration change in its reference frame,  $\partial C_N/\partial t = N(\mu, \sigma^2)$ . This stochastic measurement is normally distributed with mean  $\mu = \mathbf{v} \cdot \nabla C$  and standard deviation  $\sigma = \Pi [3C(\mathbf{x}, t)/\pi a D T^3]^{1/2}$ , and therefore directly incorporates the fundamental precision with which a cell can measure the gradient. Here  $\Pi$  is the chemotactic precision factor and  $T$  is the timescale over which the bacteria measure the gradient (see ref. <sup>32</sup>). For each bacterium, we model an internal state variable,  $S(t)$ , which evolves according to

$$\frac{dS}{dt} = -\frac{S}{t_M} + \kappa N(\mu, \sigma^2), \quad (9)$$

where  $t_M = 1.3 \text{ s}$  is the adaptation timescale<sup>50</sup> and  $\kappa$  is the effective receptor gain—the receptor gain rescaled by the half-saturation constant (see ref. <sup>32</sup>). The cell's mean run time is modified according to the following equation:

$$\tau(S) = \frac{2\tau_0}{1 + \exp(-\Gamma S)} \quad (10)$$

where  $\tau_0$  is the mean run time of bacteria in their fully adapted state and  $\Gamma$  is the (constant) dimensionless flagellar motor gain. During each timestep, the probability of re-orientation is given by  $\Delta t/\tau$ .

Run-reverse-flick re-orientation dynamics were included explicitly using known parameters derived for *Vibrio alginolyticus*<sup>51</sup>, and rotational diffusion with  $D_r = 0.0349 \text{ rad}^2 \text{ s}^{-1}$  perturbed the swimming direction at each timestep. Cell motility occurs in three dimensions, as in experiments, with swimming bacteria subject to periodic boundary conditions. The sensory integration timescale is given as  $T = 0.1 \text{ s}$ , the cell radius is taken to be  $a = 0.5 \mu\text{m}$ , the swimming speed  $v = |\nu| = 45 \mu\text{m s}^{-1}$ , and we use the diffusivity for glutamate,  $D = 608 \mu\text{m}^2 \text{ s}^{-1}$ . For the WT cells, we utilize the recently measured parameter for *Vibrio ordalii*,  $\Pi_{\text{sim}} = 6.6$ . Initially seeded randomly within the domain, we simulated the 3D motion of 500 bacteria as they respond to the DOM landscape. Within the context of this model, it is straightforward to simulate non-chemotactic ( $\Delta cheA$ ) or non-motile ( $\Delta fliC$ ) mutants by fixing  $\tau = \tau_0$  or  $\nu = 0$  respectively. We considered the same concentrations of phytoplankton cells ( $10^3, 10^4$  and  $10^5 \text{ cells ml}^{-1}$ ) as used in the experiments.

### DOM uptake by model bacteria

The bacterial trajectories from the numerical simulations were cross-referenced against the 3D DOM landscape to reveal the time series of DOM exposure for all model bacteria. Diffusion-limited uptake is proportional to the DOM concentration, and so acts as an effective proxy for actual uptake. We investigate the DOM exposure, averaged over time and across the population, as a function of DOM leakage rate and concentration of phytoplankton. The results in Extended Data Fig. 7a,b illustrate the results for non-chemotactic ( $\Delta cheA$ ) and chemotactic (WT) cells, respectively. Cells in the  $\Delta cheA$  strain swim randomly, and therefore sample all areas of their environment with equal probability. The average DOM exposure is therefore proportional to the product  $L \times \rho$  for low hotspot concentrations, a feature reflected in the straight-line level contours of Extended Data Fig. 7a. These contours are distorted in the case of WT cells (Extended Data Fig. 7b), which are able to respond to chemical gradients and attain a relatively high DOM exposure, particularly at low hotspot concentrations. Figure 4 in the main text is calculated by taking the ratio of Extended Data Fig. 7b and Extended Data Fig. 7a, directly quantifying the advantage due to chemotaxis.

We calibrated the leakage rate in the mathematical model using the following method. For each phytoplankton concentration ( $10^3, 10^4$  and  $10^5 \text{ cells ml}^{-1}$ ) and across a fine mesh of  $L$  values, we calculated the ratio of the mean DOM uptake for the WT cells compared with the  $\Delta cheA$  mutants. The value  $L = 0.052 \text{ pmol h}^{-1}$  resulted in the closest agreement between the numerical simulations (Extended Data Fig. 2) and experimental measurements (Fig. 2b). This value of  $L$  was applied in simulations designed to mimic experimental conditions.

The mathematical model does not simulate the release of  $^{13}\text{C}$ -enriched compounds from *M. adhaerens*, or subsequent uptake by *Synechococcus* cells. Nevertheless, the dynamic results of the numerical simulations provide insight into the experimental findings of Fig. 2c. For  $\rho = 10^3 \text{ cells ml}^{-1}$ , the  $^{13}\text{C}$  uptake is significantly higher for WT cells than for  $\Delta cheA$  and  $\Delta fliC$  strains, demonstrating that bacteria–phytoplankton spatial associations influence the  $^{13}\text{C}$  transfer. Interestingly, however, the  $^{13}\text{C}$  uptake in *Synechococcus* does not vary significantly with concentration of suspended *Synechococcus* cells, even though the concentration of *M. adhaerens* is constant across all treatments ( $10^6 \text{ cells ml}^{-1}$ ). If the  $^{13}\text{C}$  exchange was dominated by bulk background concentration of  $^{13}\text{C}$ -enriched *Marinobacter* exudates, then the measured enrichment would decrease with *Synechococcus* concentration, as more cells compete for fixed supply of DOM. Similarly, if *Synechococcus*-derived chemical gradients were strong enough to trap bacteria for sustained periods of time, then the  $^{13}\text{C}$  enrichment would also be expected to drop with increasing *Synechococcus* concentration,  $\rho$ . The insensitivity of the results to  $\rho$  is consistent with the physical model of fleeting bacteria–phytoplankton interactions. Since chemotaxis prolongs the bacteria–phytoplankton interactions

by only a few seconds on average, the number of bacteria entering and departing a given analysis zone per unit time—and therefore the  $^{13}\text{C}$  uptake in *Synechococcus*—is only weakly affected by the *Synechococcus* concentration itself.

For any individual *Synechococcus* cell, the associated DOM concentration profile converges to zero in the limit as  $r \rightarrow \infty$  (equation (7)). However, because the simulation volume contains multiple *Synechococcus* cells, the minimum nutrient concentration in the domain—which is found approximately midway between cells—is non-zero. We examined our simulation data to identify the lowest ('background') concentration in each treatment and found that the range of concentrations is commensurate with average free amino acid concentrations in the ocean ( $\sim 10\text{--}20 \text{ nM}$  average, with concentrations up to  $100 \text{ s or } 1,000 \text{ nM}$  in bloom conditions<sup>52,53</sup>).

Specifically, the lowest local nutrient concentration occurs in the treatments with  $10^3 \text{ Synechococcus cells ml}^{-1}$ , since the phycospheres are most widely separated. For non-chemotactic cells in this case—which explore the landscape uniformly—simulated bacterial trajectories reveal the average nutrient concentration experienced by bacteria to be  $3.7 \text{ nM}$  (averaged over the simulation time). Conversely, the maximum value of the background concentration occurs in the treatments with  $10^5 \text{ Synechococcus cells ml}^{-1}$ . We examined the simulation data corresponding to these treatments and found nutrient concentrations of approximately  $200 \text{ nM}$ , a value that is commensurate with free amino acid concentrations occurring in bloom conditions.

### Bacteria–phytoplankton dynamic interactions

The full trajectories of all model bacteria are recorded in the simulations. This facilitates exploration of the dynamic interactions between DOM sources and model bacteria. The region immediately surrounding a phytoplankton cell rich in phytoplankton exudates is known as the phycosphere<sup>9</sup>. The exact definition of the phycosphere remains challenging, since the phycosphere is composed of a wide range of chemicals, with different concentrations and diffusivities, which can be used by bacteria as either growth substrates or signals. One way to operationally define the phycosphere is through a threshold DOM concentration compared to the background value<sup>12</sup>. As our work focuses on chemotaxis, we instead define the phycosphere on the basis of the chemotactic properties of WT bacteria, and the behavioural associations with individual phytoplankton. We determine the effective phycosphere radius of the *Synechococcus* cell by examining the behavioural properties of model bacteria as a function of distance from the *Synechococcus* cell. We calculate the residence time,  $\tau$ , of bacteria within a distance  $d (\mu\text{m})$  of a *Synechococcus* cell. For WT bacteria, the rate at which this residence time increases with  $d$  is greatest for  $d \leq 35 \mu\text{m}$  (Extended Data Fig. 3), demonstrating that, within this zone, chemotaxis allows bacteria to prolong their spatial association with *Synechococcus*. Conversely, non-chemotactic cells ( $\Delta cheA$ ) exhibit a residence time that grows linearly with  $d$  at all distances, with no behavioural biases. We utilize the value  $d = 35 \mu\text{m}$  for the phycosphere radius throughout the manuscript. Crucially, the specific choice of phycosphere radius does not influence the total DOM exposure by model bacteria (and does not enter the actual simulations), only the statistics of encounters with phycospheres and time spent within them.

At every instant in time and for each bacterium, we calculate the distance to the nearest hotspot. The results in Extended Data Fig. 8a show the time- and population-averaged minimum distance, as a function of DOM leakage rate,  $L$ . The leakage rate may be approximated as scaling with cell radius according to  $L \propto r^{2.28}$  (refs. <sup>54,55</sup>). By matching the fitted leakage rate for *Synechococcus* ( $L = 0.052 \text{ pmol h}^{-1}$ ) with its known cell radius (Supplementary Table 8), leakage rate (horizontal axis of Extended Data Fig. 8a) can instead be recast in terms of cell radius. As the leakage rate  $L$  is increased, WT bacteria are increasingly able to detect and respond to the chemical gradients, resulting in closer physical association with the phytoplankton cells. The grey vertical

line in Extended Data Fig. 8a corresponds to the fitted value  $L = 0.052 \text{ pmol h}^{-1}$ .

Extended Data Fig. 8b displays the percentage of the bacterial population within a distance of 35  $\mu\text{m}$  from a hotspot. The role of chemotaxis is clear, with the fraction of cells co-localized with DOM sources increasing dramatically with DOM leakage rate. At the highest leakage rate studied, more than 85% of chemotactic bacteria are within 35  $\mu\text{m}$  of a phytoplankton cell. This percentage plateaus at a value less than 100% since the stochastic nature of bacterial run-reverse-flick motion (mean run distance  $\sim 21 \mu\text{m}$ ) precludes a cell from residing indefinitely within the analysis zone.

## Reporting summary

Further information on research design is available in the Nature Portfolio Reporting Summary linked to this article.

## Data availability

All chemotaxis, growth, metabolomics and NanoSIMS data are available at Zenodo (<https://zenodo.org/record/7509161#.Y7fUcRVBw2w>; <https://doi.org/10.5281/zenodo.7509161>). Source data are provided with this paper.

## Code availability

All analysis scripts are available on GitHub (<https://github.com/JB-Raina-codes/Synechococcus-paper>).

## References

1. Aylward, F. O. et al. Microbial community transcriptional networks are conserved in three domains at ocean basin scales. *Proc. Natl Acad. Sci. USA* **112**, 5443–5448 (2015).
2. Fuhrman, J. A. Microbial community structure and its functional implications. *Nature* **459**, 193–199 (2009).
3. Amin, S. A., Parker, M. S. & Armbrust, E. V. Interactions between diatoms and bacteria. *Microbiol. Mol. Biol. Rev.* **76**, 667–684 (2012).
4. Mayali, X. Metabolic interactions between bacteria and phytoplankton. *Front. Microbiol.* **9**, 727 (2018).
5. Amin, S. A. et al. Photolysis of iron–siderophore chelates promotes bacterial–algal mutualism. *Proc. Natl Acad. Sci. USA* **106**, 17071–17076 (2009).
6. Amin, S. A. et al. Interaction and signalling between a cosmopolitan phytoplankton and associated bacteria. *Nature* **522**, 98 (2015).
7. Durham, B. P. et al. Cryptic carbon and sulfur cycling between surface ocean plankton. *Proc. Natl Acad. Sci. USA* **112**, 453 (2015).
8. Stocker, R. Marine microbes see a sea of gradients. *Science* **338**, 628 (2012).
9. Bell, W. & Mitchell, R. Chemotactic and growth responses of marine bacteria to algal extracellular products. *Biol. Bull.* **143**, 265–277 (1972).
10. Azam, F. & Ammerman, J. W. in *Flows of Energy and Materials in Marine Ecosystems* 345–360 (Springer, 1984).
11. Mitchell, J. G., Okubo, A. & Fuhrman, J. A. Microzones surrounding phytoplankton form the basis for a stratified marine microbial ecosystem. *Nature* **316**, 58–59 (1985).
12. Seymour, J. R., Amin, S. A., Raina, J.-B. & Stocker, R. Zooming in on the phycosphere: the ecological interface for phytoplankton–bacteria relationships. *Nat. Microbiol.* **2**, 17065 (2017).
13. Sonnenschein, E. C., Syit, D. A., Grossart, H.-P. & Ullrich, M. S. Chemotaxis of *Marinobacter adhaerens* and its impact on attachment to the diatom *Thalassiosira weissflogii*. *Appl. Environ. Microbiol.* **78**, 6900–6907 (2012).
14. Raina, J.-B., Fernandez, V., Lambert, B., Stocker, R. & Seymour, J. R. The role of microbial motility and chemotaxis in symbiosis. *Nat. Rev. Microbiol.* **17**, 284–294 (2019).
15. Seymour, J. R., Ahmed, T., Durham, W. M. & Stocker, R. Chemotactic response of marine bacteria to the extracellular products of *Synechococcus* and *Prochlorococcus*. *Aquat. Microb. Ecol.* **59**, 161–168 (2010).
16. Smriga, S., Fernandez, V. I., Mitchell, J. G. & Stocker, R. Chemotaxis toward phytoplankton drives organic matter partitioning among marine bacteria. *Proc. Natl Acad. Sci. USA* **113**, 1576–1581 (2016).
17. Flombaum, P., Wang, W.-L., Primeau, F. W. & Martiny, A. C. Global picophytoplankton niche partitioning predicts overall positive response to ocean warming. *Nat. Geosci.* **13**, 116–120 (2020).
18. Christie-Oleza, J. A., Sousoni, D., Lloyd, M., Armengaud, J. & Scanlan, D. J. Nutrient recycling facilitates long-term stability of marine microbial phototroph–heterotroph interactions. *Nat. Microbiol.* **2**, 17100 (2017).
19. Morris, J. J., Kirkegaard, R., Szul, M. J., Johnson, Z. I. & Zinser, E. R. Facilitation of robust growth of *Prochlorococcus* colonies and dilute liquid cultures by ‘helper’ heterotrophic bacteria. *Appl. Environ. Microbiol.* **74**, 4530–4534 (2008).
20. Sher, D., Thompson, J. W., Kashtan, N., Croal, L. & Chisholm, S. W. Response of *Prochlorococcus* ecotypes to co-culture with diverse marine bacteria. *ISME J.* **5**, 1125–1132 (2011).
21. Aharonovich, D. & Sher, D. Transcriptional response of *Prochlorococcus* to co-culture with a marine *Alteromonas*: differences between strains and the involvement of putative infochemicals. *ISME J.* **10**, 2892–2906 (2016).
22. Jackson, G. A. Simulating chemosensory responses of marine microorganisms. *Limnol. Oceanogr.* **32**, 1253–1266 (1987).
23. Gärdes, A., Iversen, M. H., Grossart, H.-P., Passow, U. & Ullrich, M. S. Diatom-associated bacteria are required for aggregation of *Thalassiosira weissflogii*. *ISME J.* **5**, 436–445 (2011).
24. Al-Wahaib, D., Al-Bader, D., Al-Shaikh Abdou, D. K., Eliyas, M. & Radwan, S. S. Consistent occurrence of hydrocarbonoclastic *Marinobacter* strains in various cultures of picocyanobacteria from the Arabian Gulf: promising associations for biodegradation of marine oil pollution. *J. Mol. Microbiol. Biotechnol.* **26**, 261–268 (2016).
25. Raina, J.-B. et al. Subcellular tracking reveals the location of dimethylsulfoniopropionate in microalgae and visualises its uptake by marine bacteria. *eLife* **6**, e23008 (2017).
26. Brumley, D. R. et al. Cutting through the noise: bacterial chemotaxis in marine microenvironments. *Front. Mar. Sci.* **7**, 527 (2020).
27. Gärdes, A. et al. Complete genome sequence of *Marinobacter adhaerens* type strain (HP15), a diatom-interacting marine microorganism. *Stand. Genom. Sci.* **3**, 97–107 (2010).
28. Moore, L. R., Post, A. F., Rocap, G. & Chisholm, S. W. Utilization of different nitrogen sources by the marine cyanobacteria *Prochlorococcus* and *Synechococcus*. *Limnol. Oceanogr.* **47**, 989–996 (2002).
29. Wawrik, B., Callaghan, A. V. & Bronk, D. A. Use of inorganic and organic nitrogen by *Synechococcus* spp. and diatoms on the West Florida shelf as measured using stable isotope probing. *Appl. Environ. Microbiol.* **75**, 6662–6670 (2009).
30. Lambert, B. S. et al. A microfluidics-based in situ chemotaxis assay to study the behaviour of aquatic microbial communities. *Nat. Microbiol.* **2**, 1344–1349 (2017).
31. Raina, J.-B. et al. Chemotaxis shapes the microscale organization of the ocean’s microbiome. *Nature* **605**, 132–138 (2022).
32. Brumley, D. R. et al. Bacteria push the limits of chemotactic precision to navigate dynamic chemical gradients. *Proc. Natl Acad. Sci. USA* **116**, 10792–10797 (2019).
33. Myklestad, S. M. in *Marine Chemistry* (ed. Wangersky, P. J.) 111–148 (Springer Berlin Heidelberg, 2000).

34. Ni, B., Colin, R., Link, H., Endres, R. G. & Sourjik, V. Growth-rate dependent resource investment in bacterial motile behavior quantitatively follows potential benefit of chemotaxis. *Proc. Natl Acad. Sci. USA* **117**, 595–601 (2020).
35. Stocker, R., Seymour, J. R., Samadani, A., Hunt, D. E. & Polz, M. F. Rapid chemotactic response enables marine bacteria to exploit ephemeral microscale nutrient patches. *Proc. Natl Acad. Sci. USA* **105**, 4209–4214 (2008).
36. Buitenhuis, E. et al. MAREDAT: towards a world atlas of MARine Ecosystem DATa. *Earth Syst. Sci. Data* **5**, 227–239 (2013).
37. Raina, J.-B. et al. Symbiosis in the microbial world: from ecology to genome evolution. *Biol. Open* **7**, bio032524 (2018).
38. Giardina, M. et al. Quantifying inorganic nitrogen assimilation by *Synechococcus* using bulk and single-cell mass spectrometry: a comparative study. *Front. Microbiol.* **9**, 2847 (2018).
39. Berges, J. A., Franklin, D. J. & Harrison, P. J. Evolution of an artificial seawater medium: improvements in enriched seawater, artificial water over the last two decades. *J. Phycol.* **37**, 1138–1145 (2001).
40. Guillard, R. R. L. in *Culture of Marine Invertebrate Animals: Proceedings—1st Conference on Culture of Marine Invertebrate Animals* Greenport (eds Walter, L. S. & Matoira, H. C.) 29–60 (Springer US, 1975).
41. Kaeppel, E. C., Gärdes, A., Seebah, S., Grossart, H.-P. & Ullrich, M. S. *Marinobacter adhaerens* sp. nov., isolated from marine aggregates formed with the diatom *Thalassiosira weissflogii*. *Int. J. Syst. Evolut. Microbiol.* **62**, 124–128 (2012).
42. Sonnenschein, E. C. et al. Development of a genetic system for *Marinobacter adhaerens* HP15 involved in marine aggregate formation by interacting with diatom cells. *J. Microbiol. Methods* **87**, 176–183 (2011).
43. Marie, D., Partensky, F., Jacquet, S. & Vaulot, D. Enumeration and cell cycle analysis of natural populations of marine picoplankton by flow cytometry using the nucleic acid stain SYBR Green I. *Appl. Environ. Microbiol.* **63**, 186–193 (1997).
44. Schindelin, J. et al. Fiji: an open-source platform for biological-image analysis. *Nat. Methods* **9**, 676–682 (2012).
45. Hillion, F., Kilburn, M., Hoppe, P., Messenger, S. & Weber, P. K. The effect of QSA on S, C, O and Si isotopic ratio measurements. *Geochim. Cosmochim. Acta* **72**, A377 (2008).
46. Popa, R. et al. Carbon and nitrogen fixation and metabolite exchange in and between individual cells of *Anabaena oscillarioides*. *ISME J.* **1**, 354–360 (2007).
47. Sumner, L. W. et al. Proposed minimum reporting standards for chemical analysis. *Metabolomics* **3**, 211–221 (2007).
48. Clerc, E. E., Raina, J.-B., Lambert, B. S., Seymour, J. & Stocker, R. In situ chemotaxis assay to examine microbial behavior in aquatic ecosystems. *JoVE* <https://doi.org/10.3791/61062> (2020).
49. Ihaka, R. & Gentleman, R. R: a language for data analysis and graphics. *J. Comput. Graph. Stat.* **5**, 299–314 (1996).
50. Xie, L., Lu, C. & Wu, X.-L. Marine bacterial chemoresponse to a stepwise chemoattractant stimulus. *Biophys. J.* **108**, 766–774 (2015).
51. Son, K., Guasto, J. S. & Stocker, R. Bacteria can exploit a flagellar buckling instability to change direction. *Nat. Phys.* **9**, 494–498 (2013).
52. Lee, C. & Bada, J. L. Amino acids in equatorial Pacific Ocean water. *Earth Planet. Sci. Lett.* **26**, 61–68 (1975).
53. Yamashita, Y. & Tanoue, E. Distribution and alteration of amino acids in bulk DOM along a transect from bay to oceanic waters. *Mar. Chem.* **82**, 145–160 (2003).
54. Menden-Deuer, S. & Lessard, E. J. Carbon to volume relationships for dinoflagellates, diatoms, and other protist plankton. *Limnol. Oceanogr.* **45**, 569–579 (2000).
55. Mullin, M. M., Sloan, P. R. & Eppley, R. W. Relationship between carbon content, cell volume and area in phytoplankton. *Limnol. Oceanogr.* **11**, 307–311 (1966).

## Acknowledgements

The authors thank F. Carrara and A. Hein for useful discussions. This work was supported by an Australian Research Council grant (DP180100838) to J.R.S. and J.-B.R. J.-B.R. was supported by an Australian Research Council Fellowship (FT210100100). D.R.B. was supported by an Australian Research Council Fellowship (DE180100911). D.R.B. performed simulations using The University of Melbourne's High-Performance Computer Spartan (<https://doi.org/10.4225/49/58ead90dceaaa>). R.S. acknowledges support from a grant by the Simons Foundation (542395) as part of the Principles of Microbial Ecosystems Collaborative (PriME), a Gordon and Betty Moore Symbiosis in Aquatic Ecosystems Initiative Investigator Award (GBMF9197; <https://doi.org/10.37807/GBMF9197>) and a grant from the Swiss National Science Foundation (315230\_176189). We acknowledge use of the Microscopy Australia Ion Probe Facility at The University of Western Australia, a facility funded by the University, State and Commonwealth Governments. This project used NCRIS-enabled Metabolomics Australia infrastructure at the University of Melbourne, funded through BioPlatforms Australia.

## Author contributions

J.-B.R., D.R.B., S.S., R.S. and J.R.S. designed the experiments. M.G. and J.-B.R. conducted the experimental work. M.G., P.L.C., P.G. and J.B. conducted the NanoSIMS work. J.-B.R. and H.M. conducted the metabolomics. D.R.B. conducted the agent-based simulations. E.C.S. and M.S.U. provided the bacterial strains and mutants. J.-B.R., D.R.B., R.S. and J.R.S. wrote the manuscript, and all authors edited subsequent versions.

## Competing interests

The authors declare no competing interests.

## Additional information

**Extended data** is available for this paper at <https://doi.org/10.1038/s41564-023-01327-9>.

**Supplementary information** The online version contains supplementary material available at <https://doi.org/10.1038/s41564-023-01327-9>.

**Correspondence and requests for materials** should be addressed to Jean-Baptiste Raina or Justin R. Seymour.

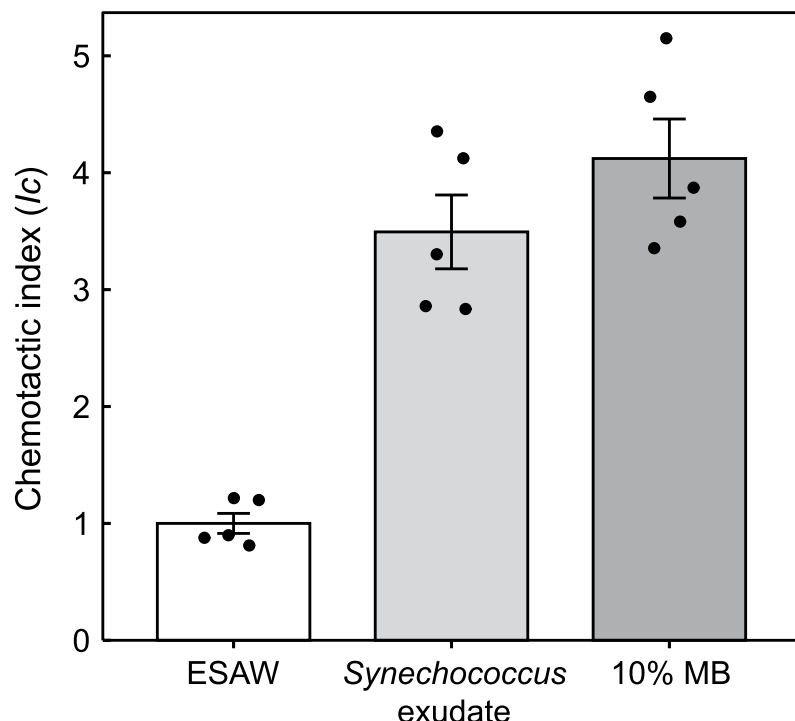
**Peer review information** *Nature Microbiology* thanks Simon van Vliet and the other, anonymous, reviewer(s) for their contribution to the peer review of this work.

**Reprints and permissions information** is available at [www.nature.com/reprints](http://www.nature.com/reprints).

**Publisher's note** Springer Nature remains neutral with regard to jurisdictional claims in published maps and institutional affiliations.

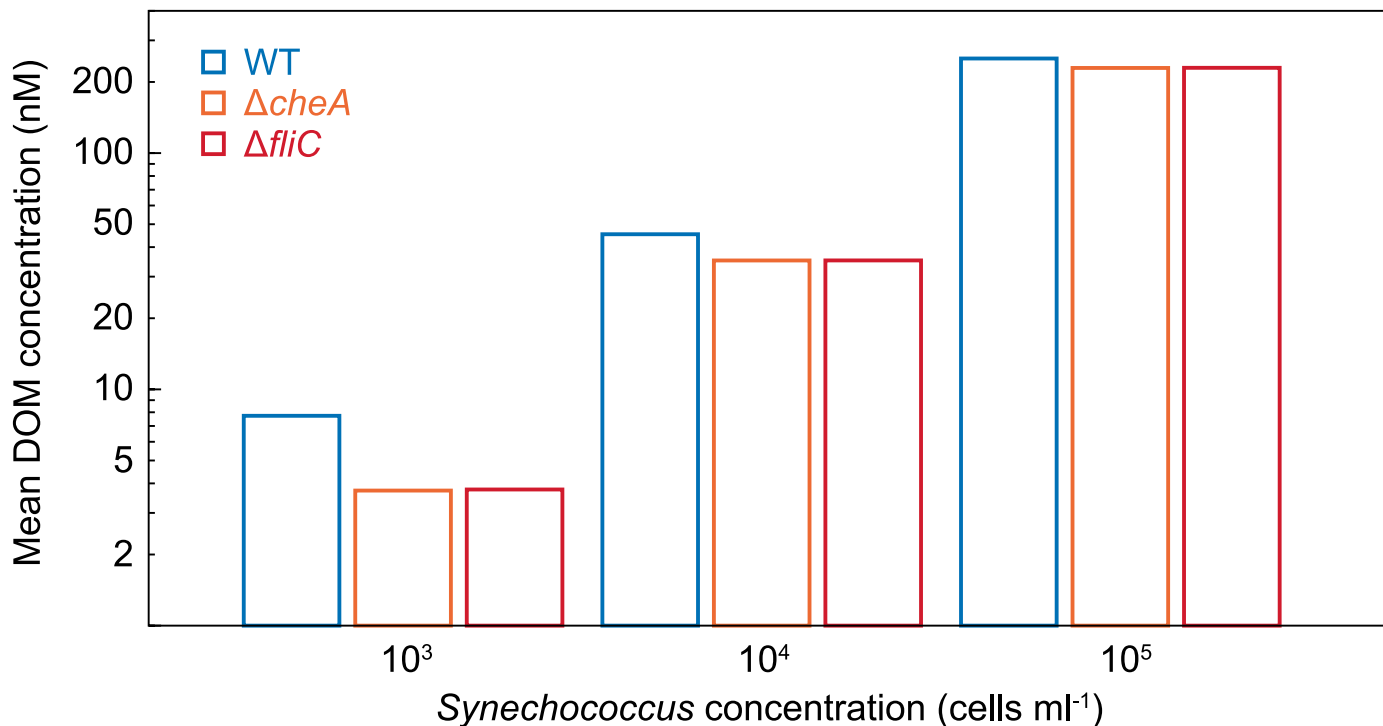
Springer Nature or its licensor (e.g. a society or other partner) holds exclusive rights to this article under a publishing agreement with the author(s) or other rightsholder(s); author self-archiving of the accepted manuscript version of this article is solely governed by the terms of such publishing agreement and applicable law.

© The Author(s), under exclusive licence to Springer Nature Limited 2023



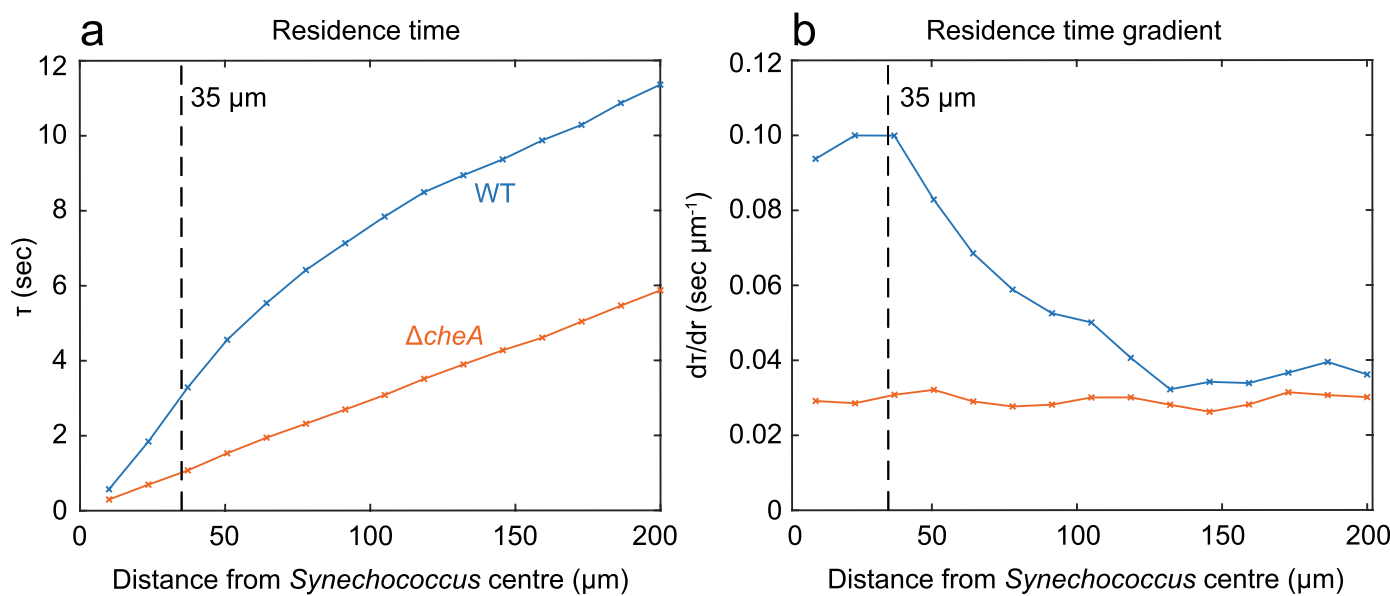
**Extended Data Fig. 1 | Chemotactic response of *Marinobacter adhaerens* HP15 to metabolites exuded by *Synechococcus*.** The chemotactic index,  $I_c$  denotes the concentration of cells within ISCA wells, normalized by the mean concentration of cells within wells containing no chemoattractants (filtered ESW), after 30 min laboratory deployment. Wells containing *Synechococcus*

exudates (1 mg ml<sup>-1</sup>) and 10% Marine Broth (MB) contained significantly more bacteria than the ESW control (ANOVA,  $n = 5$  biologically independent samples,  $p < 0.005$ ; Supplementary Table S). Error bars represent standard error of the mean.

**Extended Data Fig. 2 | Dissolved Organic Matter (DOM) exposure of model**

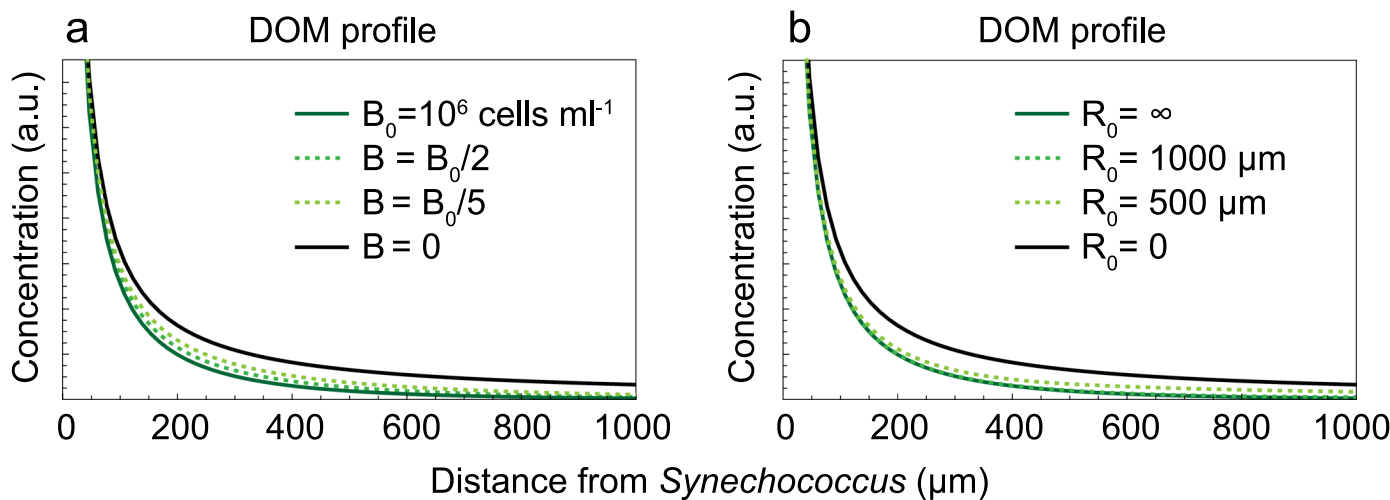
**bacteria.** Mean DOM exposure for three bacterial motility strategies across three different *Synechococcus* concentrations (leakage rate  $L = 0.052 \text{ pmol hr}^{-1}$ ). Chemotaxis conferred an enhancement in the DOM exposure by 2.1-, 1.3-, and

1.1-fold, for *Synechococcus* concentrations of  $10^3$ ,  $10^4$ , and  $10^5 \text{ cells ml}^{-1}$  respectively, compared to non-chemotactic ( $\Delta cheA$ ) or non-motile ( $\Delta fliC$ ) mutants.



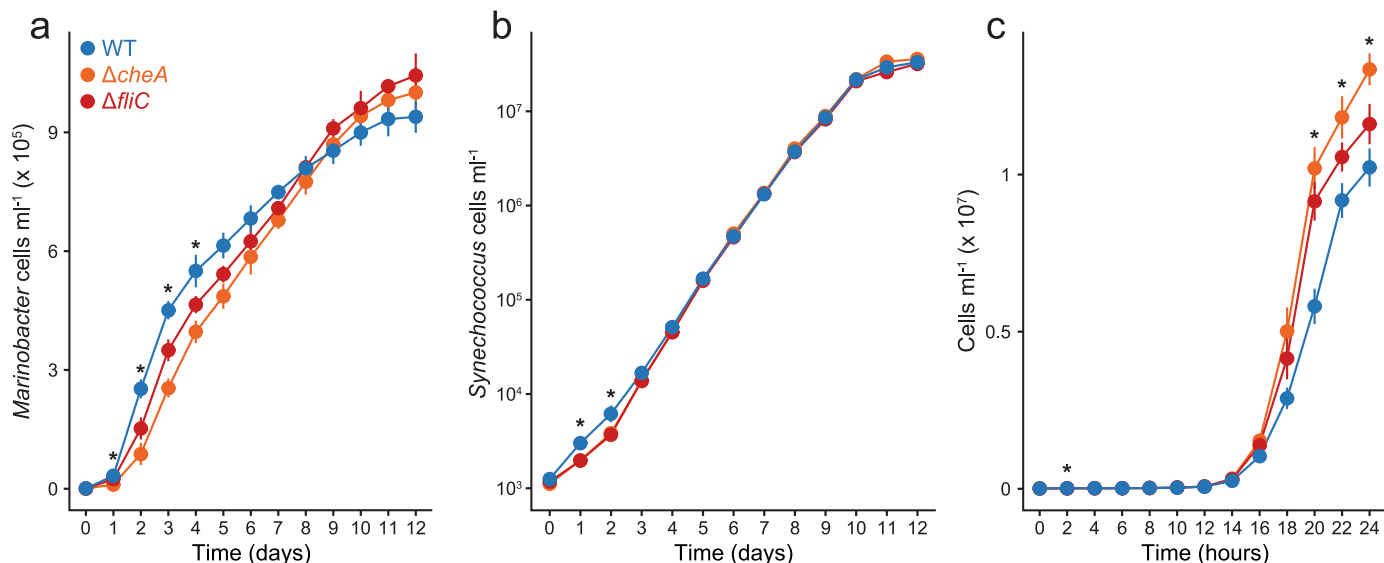
**Extended Data Fig. 3 | Residence time of model bacteria.** (a) The bacterial residence time depends on the radius of the analysis zone and motility strategy. For  $\Delta\text{cheA}$  mutants, the residence time grows linearly with radius. However, WT cells exhibit a steep increase for small radii, reflecting their capacity to detect the phytoplankton exudates. (b) The rate at which the residence time increases with

radius reveals the zone in which chemotactic bacteria exhibit the strongest behavioral response to the DOM gradient. From this the encounter radius of  $35 \mu\text{m}$  can be extracted. Other model parameters include  $L = 0.052 \text{ pmol hr}^{-1}$ ,  $\rho = 10^3 \text{ cells ml}^{-1}$ .



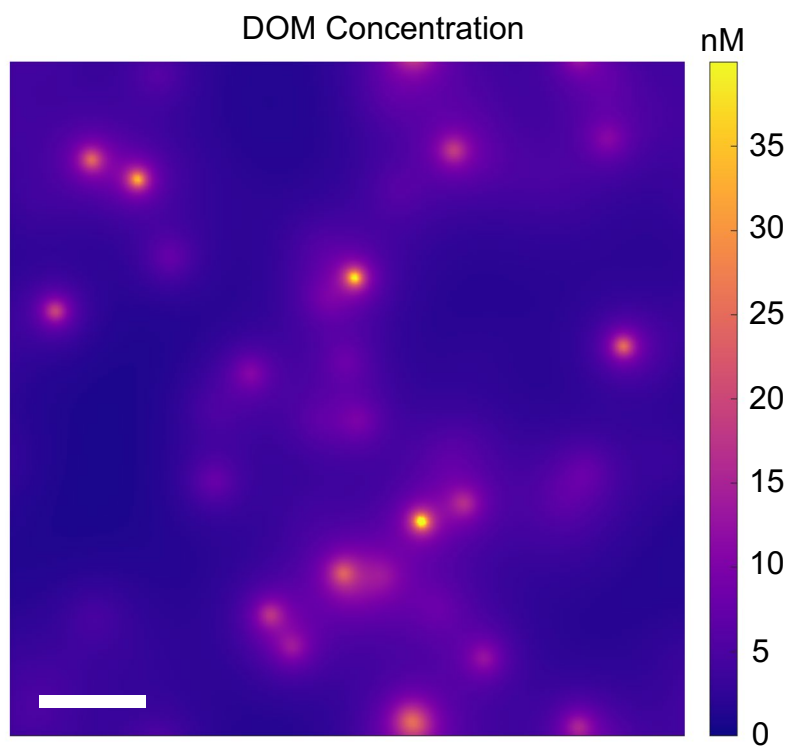
**Extended Data Fig. 4 | DOM profile does not depend strongly on bacterial consumption.** In each plot, the steady state DOM profile emerges due to a balance between constant phytoplankton exudation and diffusion-limited

uptake by bacteria. **(a)** DOM profile for four different bacterial concentrations. **(b)** Restricting bacteria to lie in the region  $R < R_0$  has a minor influence on the resultant DOM profile.

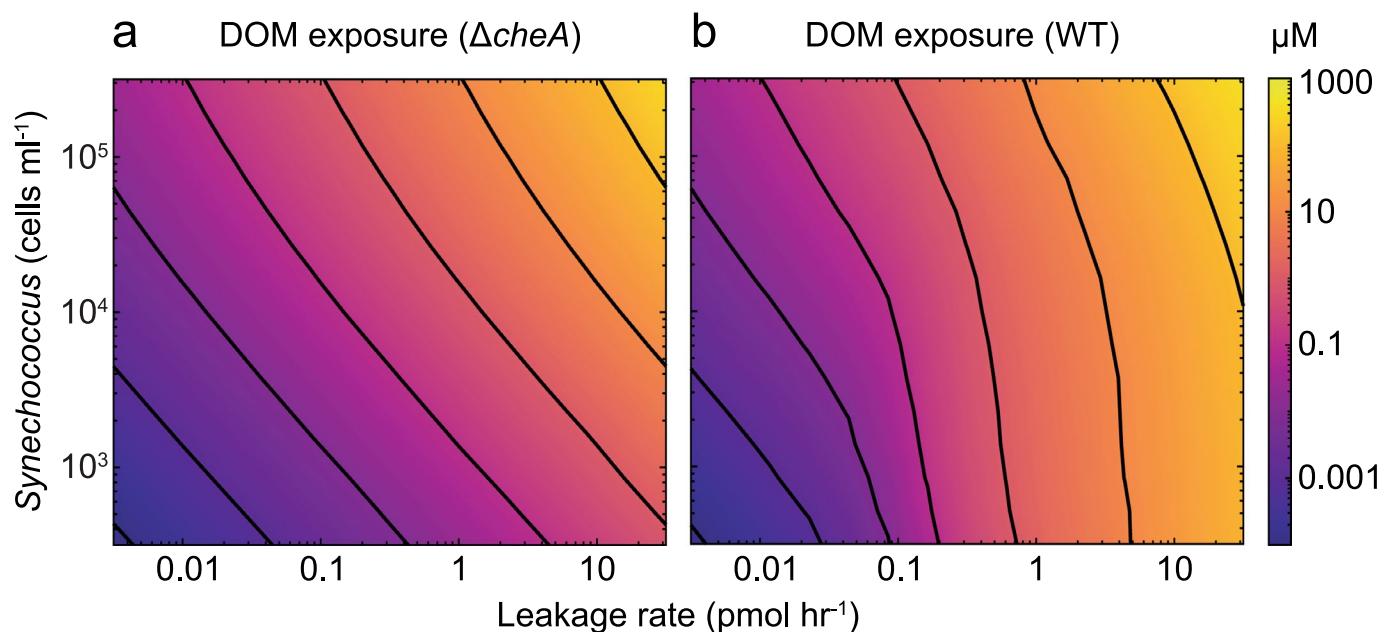


**Extended Data Fig. 5 | Growth of *Synechococcus* sp. CS-94 RRIMP N1 and *Marinobacter adhaerens* HP15.** (a) Growth curves of *M. adhaerens* HP15 wild type (WT), non-chemotactic mutant ( $\Delta$ cheA), and non-motile mutant ( $\Delta$ fliC), each separately co-cultured with *Synechococcus* at an initial concentration of  $10^3$  cells ml<sup>-1</sup> for both partners. (b) Simultaneous growth curve of *Synechococcus* for the same three co-culture experiments. Note: to clearly visualise differences in cell numbers during early timepoints, *Synechococcus* cell numbers are plotted on a logarithmic scale. Asterisks indicate timepoints at which treatments are

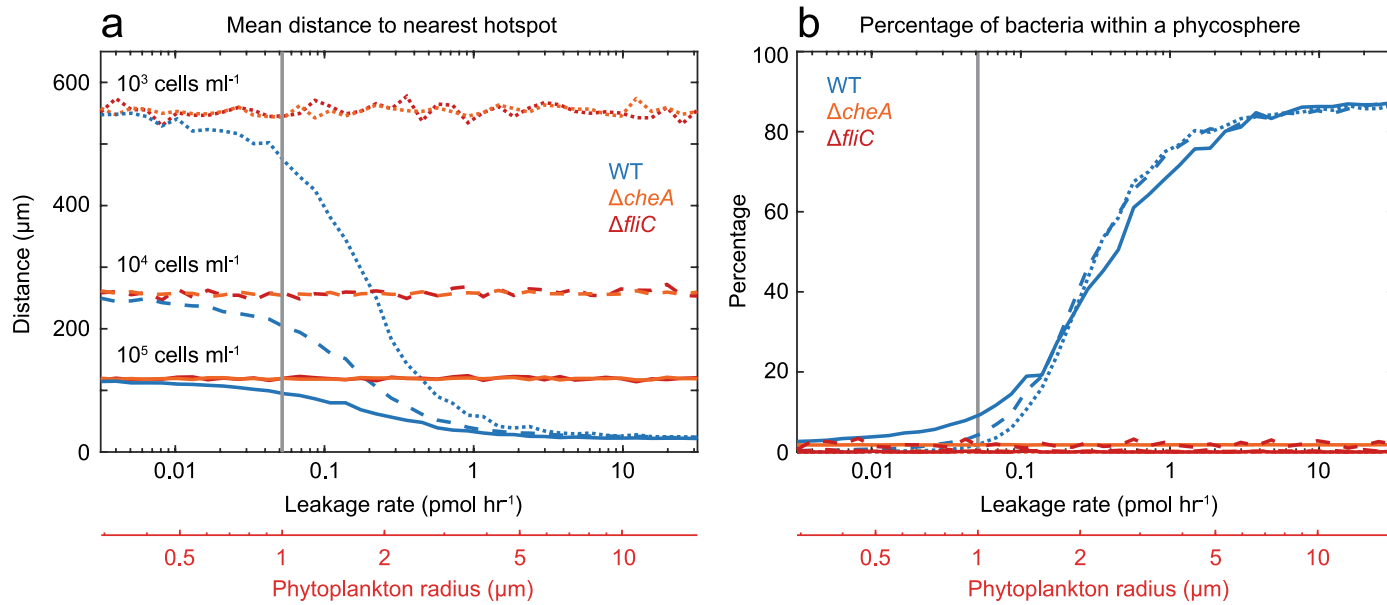
significantly different (simple main effect test,  $p < 0.05$ , Supplementary Table 9). Error bars represent standard error of the mean ( $n = 4$  biologically independent samples). (c) Growth curves of *Marinobacter adhaerens* HP15 wild type (WT), non-chemotactic mutant ( $\Delta$ cheA), and non-motile mutant ( $\Delta$ fliC) in Marine Broth. Error bars represent standard error of the mean ( $n = 3$  biologically independent samples). Asterisks indicate timepoints at which treatments are significantly different (simple main effect test,  $p < 0.05$ , Supplementary Table 10).



**Extended Data Fig. 6 | DOM concentration within a 2D cross-section of the full 3D profile.** Results correspond to a *Synechococcus* concentration of  $\rho = 10^3$  cells  $\text{ml}^{-1}$ . Other parameters as in Supplementary Table 8. The white scale bar represents 1 mm.

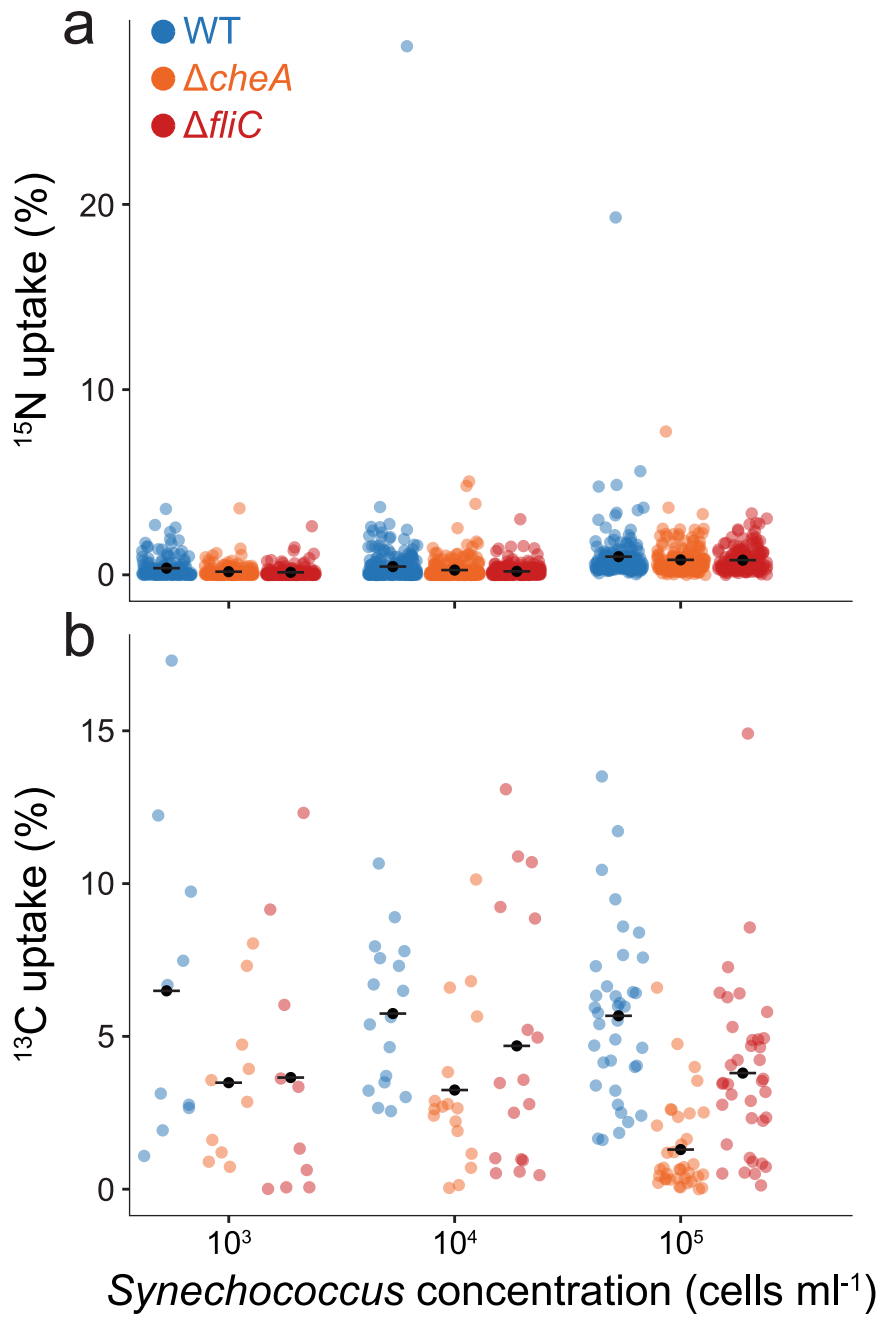


**Extended Data Fig. 7 | DOM exposure of model bacteria.** The mean DOM concentration experienced by (a) non-chemotactic ( $\Delta cheA$ ) mutants and (b) chemotactic (WT) bacteria, as a function of phytoplankton concentration (cells ml<sup>-1</sup>) and DOM leakage rate  $L$  (pmol hr<sup>-1</sup>).



**Extended Data Fig. 8 | Phytoplankton exudation rate affects bacteria-phytoplankton distances and bacterial ‘trapping’.** (a) Bacteria-phytoplankton distance is strongly affected by phytoplankton exudation rate. These data show the distance to the nearest hotspot, averaged over time (3 h co-incubation) and bacterial population (500 cells), as a function of DOM leakage rate  $L$  (pmol hr<sup>-1</sup>). Results are shown for three different phytoplankton concentrations,  $10^3$  (dotted),  $10^4$  (dashed),  $10^5$  cells ml<sup>-1</sup> (solid), and for three different bacterial mutants: chemotactic WT (blue), non-chemotactic  $\Delta cheA$  (orange), non-motile  $\Delta fliC$  (red).

ΔfliC (red). (b) Bacteria-phytoplankton trapping statistics. These data show the percentage of bacterial cells that are situated within 35 μm of a phytoplankton cell (phycosphere), as a function of DOM leakage rate  $L$  (pmol hr<sup>-1</sup>). For each datapoint, results have been averaged over time (3 h co-incubation) and bacterial population (500 cells). Results are shown for three different phytoplankton concentrations,  $10^3$  (dotted),  $10^4$  (dashed),  $10^5$  cells ml<sup>-1</sup> (solid), and for three different bacterial mutants: chemotactic WT (blue), non-chemotactic  $\Delta cheA$  (orange), non-motile  $\Delta fliC$  (red).



**Extended Data Fig. 9 | Distribution of the single cell enrichment data reported in Figs. 1 and 2.** (a)  $^{15}\text{N}$  uptake of *M. adhaerens* ( $10^3$ : n = 166;  $10^4$ : n = 286;  $10^5$ : n = 172) and (b)  $^{13}\text{C}$  uptake of *Synechococcus* ( $10^3$ : n = 10;  $10^4$ : n = 17;  $10^5$ : n = 37).

## Reporting Summary

Nature Portfolio wishes to improve the reproducibility of the work that we publish. This form provides structure for consistency and transparency in reporting. For further information on Nature Portfolio policies, see our [Editorial Policies](#) and the [Editorial Policy Checklist](#).

### Statistics

For all statistical analyses, confirm that the following items are present in the figure legend, table legend, main text, or Methods section.

n/a Confirmed

- The exact sample size ( $n$ ) for each experimental group/condition, given as a discrete number and unit of measurement
- A statement on whether measurements were taken from distinct samples or whether the same sample was measured repeatedly
- The statistical test(s) used AND whether they are one- or two-sided
  - Only common tests should be described solely by name; describe more complex techniques in the Methods section.*
- A description of all covariates tested
- A description of any assumptions or corrections, such as tests of normality and adjustment for multiple comparisons
- A full description of the statistical parameters including central tendency (e.g. means) or other basic estimates (e.g. regression coefficient) AND variation (e.g. standard deviation) or associated estimates of uncertainty (e.g. confidence intervals)
- For null hypothesis testing, the test statistic (e.g.  $F$ ,  $t$ ,  $r$ ) with confidence intervals, effect sizes, degrees of freedom and  $P$  value noted
  - Give  $P$  values as exact values whenever suitable.*
- For Bayesian analysis, information on the choice of priors and Markov chain Monte Carlo settings
- For hierarchical and complex designs, identification of the appropriate level for tests and full reporting of outcomes
- Estimates of effect sizes (e.g. Cohen's  $d$ , Pearson's  $r$ ), indicating how they were calculated

*Our web collection on [statistics for biologists](#) contains articles on many of the points above.*

### Software and code

Policy information about [availability of computer code](#)

Data collection CytExpert Version 2.4, Agilent MassHunter Qualitative and Quantitative Analysis version B.08.00, LabSolutions Insight

Data analysis Fiji Version 1.53c with Open-MIMS plug-in, statistics were carried out in R v4.1.1 and all analysis scripts are available on GitHub (<https://github.com/JB-Raina-codes/Synechococcus-paper>).

For manuscripts utilizing custom algorithms or software that are central to the research but not yet described in published literature, software must be made available to editors and reviewers. We strongly encourage code deposition in a community repository (e.g. GitHub). See the Nature Portfolio [guidelines for submitting code & software](#) for further information.

### Data

Policy information about [availability of data](#)

All manuscripts must include a [data availability statement](#). This statement should provide the following information, where applicable:

- Accession codes, unique identifiers, or web links for publicly available datasets
- A description of any restrictions on data availability
- For clinical datasets or third party data, please ensure that the statement adheres to our [policy](#)

All raw data have been deposited in Zenodo (<https://zenodo.org/record/7509161#.Y7fUcRVBw2w>); DOI: 10.5281/zenodo.7509161

## Human research participants

Policy information about [studies involving human research participants](#) and [Sex and Gender in Research](#).

Reporting on sex and gender

This is not human research

Population characteristics

This is not human research

Recruitment

This is not human research

Ethics oversight

This is not human research

Note that full information on the approval of the study protocol must also be provided in the manuscript.

## Field-specific reporting

Please select the one below that is the best fit for your research. If you are not sure, read the appropriate sections before making your selection.

Life sciences

Behavioural & social sciences

Ecological, evolutionary & environmental sciences

For a reference copy of the document with all sections, see [nature.com/documents/nr-reporting-summary-flat.pdf](https://nature.com/documents/nr-reporting-summary-flat.pdf)

## Ecological, evolutionary & environmental sciences study design

All studies must disclose on these points even when the disclosure is negative.

Study description

This study aimed to characterise the ability of heterotrophic bacteria to chemotax towards Synechococcus, quantify their uptake of Synechococcus-derived compounds and determine the impact of this enhanced nutrient exposure on their ecology. We carried out NanoSIMS experiments, chemotaxis assays, co-growth experiments, and numerical simulations, comparing wild-type cells (which are both motile and chemotactic) to mutants deficient in either motility or chemotaxis (acting as controls). Each experiment was replicated. The experiments were either one- or two-factors design.

Research sample

The research samples consisted of co-cultures with the heterotrophic bacterium Marinobacter adhaerens HP15 and Synechococcus sp. CS-94 RRIMP N1.

Sampling strategy

Pilot studies were carried out before conducting the experiment described in this manuscript. We selected our sample size based on these pilot studies, the available literature, feasibility and the variability between replicates. No statistical method was used to predetermine sample size.

Data collection

Stable isotope enrichment data were collected on a NanoSIMS 50 (Cameca, Gennevilliers, France) at the Centre for Microscopy, Characterisation and Analysis (CMCA) at The University of Western Australia. Cell counts data were recorded using CyteExpert Version 2.4. Mass spectra were collected electronically using a 72030 Shimadzu gas chromatograph and a TQ8050 quadrupole mass spectrometer (Shimadzu, Japan).

Timing and spatial scale

For stable isotope tracing, samples were collected after three hours, based on pilot studies. For chemotaxis experiments, data were collected after one hour (based on previously published protocols). For co-culture experiments, data were collected every day for twelve days (the length of the growth cycle of Synechococcus). For the growth curves of Marinobacter, data were collected every hour for 24 hours (note: replicated cultures for each treatment were set up twice 12 hours apart. The first set of cultures was enumerated for the first 10 hours, and 12 hours later, the second set of cultures was enumerated between 10 and 24 hours).

Data exclusions

No data was excluded from the study and analyses.

Reproducibility

All experiments described in the manuscript were fully replicated, with three or more biological replicates.

Randomization

Samples were allocated into groups based on the mutant identity of Marinobacter (i.e., either (1) motile and chemotactic; (2) non-motile; (3) non-chemotactic).

Blinding

Blinding was not pertinent to our study because it did not include any animals and/or human research participants. In addition, blinding was not possible since many analyses were also carried out by the persons in charge of sampling.

Did the study involve field work?

Yes       No

## Reporting for specific materials, systems and methods

We require information from authors about some types of materials, experimental systems and methods used in many studies. Here, indicate whether each material, system or method listed is relevant to your study. If you are not sure if a list item applies to your research, read the appropriate section before selecting a response.

## Materials & experimental systems

n/a	Involved in the study <input checked="" type="checkbox"/> Antibodies <input checked="" type="checkbox"/> Eukaryotic cell lines <input checked="" type="checkbox"/> Palaeontology and archaeology <input checked="" type="checkbox"/> Animals and other organisms <input checked="" type="checkbox"/> Clinical data <input checked="" type="checkbox"/> Dual use research of concern
-----	---

## Methods

n/a	Involved in the study <input checked="" type="checkbox"/> ChIP-seq <input checked="" type="checkbox"/> Flow cytometry <input checked="" type="checkbox"/> MRI-based neuroimaging
-----	---

## Flow Cytometry

### Plots

Confirm that:

- The axis labels state the marker and fluorochrome used (e.g. CD4-FITC).
- The axis scales are clearly visible. Include numbers along axes only for bottom left plot of group (a 'group' is an analysis of identical markers).
- All plots are contour plots with outliers or pseudocolor plots.
- A numerical value for number of cells or percentage (with statistics) is provided.

### Methodology

#### Sample preparation

Seawater samples derived from the In Situ Chemotaxis Assay were fixed (2% glutaraldehyde, final concentration), kept on ice and analysed the same day. Each sample was then stained with SYBR Green (1:10,000 final dilution; ThermoFisher), incubated for 15 min in the dark and analysed.

#### Instrument

CytoFLEX S (Beckman Coulter, USA) using filtered MilliQ water as sheath fluid.

#### Software

CytExpert Version 2.4

#### Cell population abundance

The target bacterial cell populations were the only ones present in the analysis plots.

#### Gating strategy

Gating around the bacterial populations was determined by pilot studies.

Tick this box to confirm that a figure exemplifying the gating strategy is provided in the Supplementary Information.